UNIVERSITY OF CALIFORNIA,

IRVINE

Nanoprobe Platform For Quantifying Gene Expression Levels in Single Living Cell

DISSERTATION

submitted in partial satisfaction of the requirements

for the degree of

DOCTOR OF PHILOSOPHY

in Material Science and Engineering

by Yinglei Tao

Dissertation Committee:

Professor H. Kumar Wickramasinghe, Chair

Professor Abraham Lee

Professor Peter Burke

2016

DEDICATION

To

my family, teachers, and friends

in recognition of their worth

TABLE OF CONTENTS

LIST OF FIGURES

Page

ACKNOWLEDGMENTS

Frist, I would like to express the deepest appreciation to my committee chair, Professor H. Kumar Wickramasinghe, for his commitment and the extraordinary support and guidance he has extended over the years. I really appreciate my advisor gave me the opportunity to work on this topic and worked very closely with me along the way. I consider myself very fortunate for learning my ropes in research from a meticulous and thought-provoking scientist like him. Without his guidance and persistent help, this dissertation would not have been possible.

Great appreciations to Prof. Abraham Lee, and Prof. Peter Burke for their generosity in making time to serve on my Ph.D. committee, in spite of their busy schedule. I would also like to thank them for their encouragement and guidance during the research as well as reviewing my dissertation. Also, I would like to thank Prof. Rahul Warrior, Prof. Han Li and Prof. Martha Mecartney for their support during the candidacy examination.

I would also like to thank our collaborators Xuan Li, Prof. Rahul Warrior, Prof. Kavita Arora, Dr.Line Hoffman and Dr. Yun Ding for their support along the way. Besides, a thank you to Prof. Philip Day at the University of Manchester, who also provided excellent suggestions to this project.

In addition, I would like to thank my lab members: Elaheh Shekaramiz, Dr. Fei Huang, Dr. Indrajith Rajapaksa, Dr. Ananth Tamma, Dr. Ganeshkumar Varadarajalu, Dr. Jonathan Burdett, Dr. Jinwei Zeng, Elaheh Shekaramiz, and Zahra Mardy, Mohsen Rajaei, Mohammad Ali Almajhadi for their support. I would also like to thank the staff at the UC Irvine

Materials Research Institute (IMRI) for their support for the materials characterization and staff from Integrated Nano Research Facility(INRF) at UCI for their support during the device fabrication. Thanks for the support from W.M. Keck Foundation for Live Cell Genomics under Grant No. KF-52356.

Finally, I would like to thank my parents for supporting me in every way during this challenging and most rewarding period of my life.

CURRICULUM VITAE

Yinglei Tao

2007 B.S. in Materials Science and Engineering,
Qingdao University of Science and Technology

2010 M.S. in Condensed Matter Physics,
Beijing Jiaotong University

2016 Ph.D. in Materials Science and Engineering,
University of California, Irvine

FIELD OF STUDY

Bioinstrumentation, Biosensor and Nanotechnology

PUBLICATIONS

Yinglei Tao, Shekarae Shekaramiz, Xuan Li and H. Kumar Wickramasinghe, "Nanoprobe platform for targeting and quantifying gene expression levels in single living cell" (in preparation)

Xuan Li*, **Yinglei Tao***, Do-Hyun Lee, H. Kumar Wickramasinghe and Abraham P. Lee, "In situ mRNA isolation from a microfluidic single-cell array using an external AFM nanoprobe" Science Advance (co-first author submitted)

Yinglei Tao and H. Kumar Wickramasinghe, "Coaxial atomic force microscope probes for dielectrophoresis of DNA under different buffer conditions" Applied Physics Letters, (under review)

Lier Deng, Ming Fu, **Yinglei Tao**, Xiaoyun Guo, "Fabrication of ordered poly (methyl methacrylate) nanobowl arrays using SiO_2 colloidal crystal templates" Journal of nanoscience and nanotechnology 14 (6), 4622 (2014)

Yinglei Tao, Ming Fu, Ailun Zhao, Dawei He and Yongsheng Wang, “The effect of seed layer on morphology of ZnO nanorod arrays grown by hydrothermal method” Journal of alloys and compounds, 489, 99 (2010)

Lier Deng, Ming Fu, Yongsheng Wang, Daeei He, Ailun Zhao, **Yinglei Tao**, Weijia Fu, "Synthesis of ordered macroporous polymers from colloidal silica templates" Journal of nanoscience and nanotechnology 10 (3), 1778 (2010)

Yinglei Tao, Ming Fu, Ailun Zhao, Dawei He and Yongsheng Wang, “Sputtering fabrication of large scale ZnO nanobowl arrays fabricated using colloidal crystal templates” Journal of nanoscience and nanotechnology 11, 7603 (2010)

Ailun Zhao, Ming Fu, **Yinglei Tao**, Lier Deng, Dawei He, Yongsheng Wang, “Cu_2O particles with ordered pores via electrochemical deposition method” Chinese Optics Letters 7 (10), 915 (2009)

Fengxian Xie, Chunjun Liang, Ziqun He, **Yinglei Tao** "Polymer photovoltaic cell using /G-PEDOT nanocomplex film as electrode" International Journal of Photoenergy 2008, Article ID 415861 (2009)

ABSTRACT OF THE DISSERTATION

Nanoprobe Platform For Quantifying Gene Expression Levels in Single Living Cell

By

Yinglei Tao

Doctor of Philosophy in Material Science and Engineering

University of California, Irvine, 2016

Professor H. Kumar Wickramasinghe, Chair

Dissecting the regulation of gene expression processes is fundamental to understand how cells function. Techniques used to obtain our current view of gene expressions rely on isolating mRNAs from large numbers of cells, which often associates with a loss or damage of the material, as well as the loss of spatial information. Also, individual cells within a population are

unlikely to behave all in the same way, and current standard techniques are unable to detect cell-to-cell differences that can result from genetic variation, biological noise and different characteristics of genes within a population.

To solve these limitations, we developed a sensitive and non-destructive method and apparatus for tracking gene expressions on single cell level within a population of cells, either on a collagen cell culture gel or in a microfluidic environment. The developed bench-top instrument utilizes a modified AFM (Atomic Force Microscopy) probes for in situ extraction of mRNA molecules from single cells. The modified coaxial AFM probe serves as nanotweezer, and wherein the application of an alternating potential between the inner and outer electrodes of the co-axial cable creates a dielectrophoretic force for attracting target molecules toward the tip-end. For adherent cell lines, the samples are cultured on collagen gel for select-and-probe analysis. An integrated microfluidic/nanoprobe platform is also developed for gene expression analysis of suspension cells on single cell level.

This system directly targets and samples down to a few molecules within a single living cell, without the need for purification and averaging typically of conventional technologies. By providing reliable and exceptional sensitivity to identify differences between individual cells in a seemingly homogeneous population, the system creates possibilities for assaying the genomic analysis in living cells and tracking them in response to external stimuli. This technique has potential impacts on understanding the heterogeneity of transcriptional responses as well as its

implications for cell function and disease. It is going to have broad application areas ranging from systems biology to cancer research.

CHAPTER 1 INTRODUCTION

In multicellular organisms, almost every cell has an identical genome, the fundamental differences between cells lie in which genes are transcribed into mRNA, i.e., their transcriptome. The unique transcriptional profile and the precise levels at which genes are expressed define individual cell fate, physiological status and behavior. To gain detailed mechanistic insights into cellular behavior, their response to signaling events and the environment, it is becoming increasingly critical to sample transcription at the single cell level.

The current gold standards for gene profiling are quantitative Real Time PCR (qRT-PCR or qPCR), microarray and RNA sequencing (RNA-seq) analysis. These techniques use reverse transcription to synthesize cDNA from mRNA and success depends on obtaining non-degraded, pure RNA samples. Furthermore, these approaches only measure average transcript levels since the mRNA is typically extracted from $>10^3$–10^6 cells. Thus, it becomes challenging when studying embryo or diagnostic analysis in diseases such as cancer where very little tissue might be available for analysis [1]. For example, a developing embryo, tissue, or tumor consists of many types of cells that may be spatially organized in complex structures. The cell types that are responsible for renewing the tissue may comprise a vanishingly small fraction of the entire tissue [2].

In this work, we developed a sensitive and non-destructive method and apparatus –the single cell analyzer for tracking gene expressions on single cell level

within a population of cells, either on a collagen cell culture gel or in a microfluidic environment. This system directly targets and samples down to a few molecules within a single living cell, without the need for purification and averaging typically of conventional technologies. The rest of the sections in this chapter will elaborate on the general background of single cell analysis and introduce the details of the single cell analyzer based on nanoprobe platform.

1.1 Cellular heterogeneity

It is becoming clear that gene expression is rather noisy at the single-cell level, both because of the small number of molecules controlling biochemical processes in the cell and the changing microenvironment [3,4]. Individual cells within a population are unlikely to behave all in the same way, and current standard techniques are unable to detect cell-to-cell differences that can result from genetic variation, biological noise and different characteristics of genes within a population. Since stochastic heterogeneity in gene expression and transcription events leads to cell-to-cell variations in a cell population, individual cells have unique characteristics, which are obscured in analyses by bulk assays [5,6], as illustrated in Figure 1.1. The single-cell analysis provides wealthy information and reveals the complex heterogeneity of cell populations, not only allowing us to interrogate fundamental cellular mechanisms but also uncovering the stochastic fluctuations among cell populations, making it crucial in biomedical researchers [7]. For example, single-cellular level genomic analysis can differentiate specific sub-

populations from clonal cell populations that exhibit diverse outcomes in response to the same stimuli [8]. On the other hand, isolated primary cells are still in a mixture of multiple types of cells due to limitations in purification protocols, to which single-cell-based screening can be utilized to detect and identify the particular cells of interest [9].

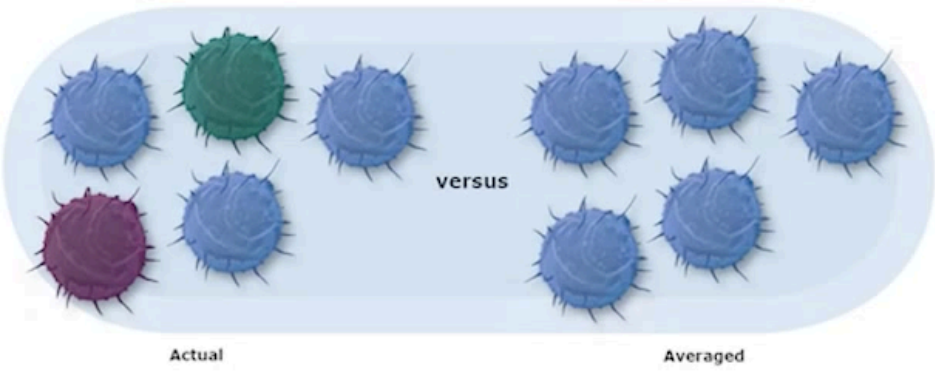

Figure 1.1 Individual cells that have unique characteristics are obscured in analyses by bulk assays

1.2 Single cell diagnostics

The heterogeneity between tumors of the same type as well as intratumor heterogeneity is integral features of cancer and the primary cause of resistance against systemic therapies [10-12]. As cancer cells shed from either primary tumors or metastatic sites [13,14], circulating tumor cells (CTCs) are gaining increasing clinical attention because they may enable the monitoring cancer progression and adjustment

of treatment. CTCs have shown promise as a real-time liquid biopsy to replace conventional tissue biopsies of metastatic tumors for cancer diagnosis, monitoring, and therapeutics [15,16]. CTCs are extremely rare, comprising as few as one cell in a background of 10^9 hematologic cells per milliliter blood of patients with metastatic cancer [14,15]. Identification of individual CTCs is, therefore, important not only to monitor intra-tumor heterogeneity from whole blood samples but also to identify target tumor cells of interest from the background of leukocytes. Although numerous high-performance microfluidic devices have been established for CTC isolation and enrichment based on the CTC counts, e.g., affinity-based capturing [17,18], magnetic isolation [19,20] and hydrodynamic separation [21,22], the sacrifice of purity of recovered CTCs remains a significant challenge due to the overlap in the size distribution of white blood cells (WBCs) and CTCs.

1.3 Current approach and technologies

Recently single cell analysis has become a hot topic of research since the development of micro/nanofluidic technologies has made it possible to automate the processing, manipulation, and analysis of populations of cells one at a time. In general, bench-top single-cell studies are limited by their high cost, low throughput as well as difficulties in analyzing small concentrations of starting materials. On the contrary, microfluidic technology requires low reagent costs and can attain high analysis efficiency [23]. With parallelization, the processes can be high throughput, automated,

and enable multi-step assays. A variety of microfluidic platforms have been developed to analyze single cells from genotype to phenotype, such as on-chip single-cell real-time PCR with a whole-process integration [9], droplet barcode-based single-cell sequencing [24], and high-density trapping arrays for single-cell imaging [25]. The Mathies group at UC Berkeley and the Quake group at Stanford have also developed single-cell mRNA analysis techniques that use microfluidic systems. Using an integrated microfluidic bioprocessor for single-cell gene expression analysis [26], the Mathies group has shown that in Jurkat cells siRNA-mediated knockdown of GAPDH expression results in two distinct cell populations – cells with partial (50%) and complete (0%) knockdown. This stochasticity in transcript number at the individual cell level is not apparent in measurements of mRNA knockdown averaged over 50 cells (21%) [27]. Quake and colleagues have used Polydimethylsiloxane (PDMS) structures and on-chip PCR to realize large-scale integration for applications in single cell mRNA isolation and analysis [28]. Quake's technology has been adopted by Fluidigm Corporation, demonstrated the commercial promise of miniaturization for single cell genomics. The Fluidigm Dynamic Array enables gene expression measurements in individual cells and represents the first dedicated commercial product for single cell analysis.

In single cell diagnosis areas, the single-cell transcriptomic analysis reveals in-depth information of cancer cell behavior and their heterogeneity according to marker gene expressions. In recent years a substantial number of microfluidic-based CTC enrichment systems have been developed that aims to provide reliable CTC detection and analysis.

Approaches based on affinity capture [29,30] magnetic isolation [31,32] size-based separation (33,34) and flow-based assays [35,36] have achieved relatively success in CTC detection and analysis.

1.4 Disadvantages and limitations in single cell analysis

Although the development of microfluidic technologies has made it possible to manipulation, and analysis of populations of cells one at a time, cell trypsinization is required for adherent cell lines or cell samples, which could alter the cell status or change gene expression profile of target samples. An in situ analysis technique is needed with the ability to maintain sample cells within their culturing network during the study. Moreover, attempts to adapt microfluidic technologies to single cell analysis have been proved challenging since lacking sensitivity, while many mRNAs are expressed at copy numbers of a few dozen per cell. Techniques such as single-cell reverse transcriptase-polymerase chain reaction (RT-PCR) can provide a closer look at RNA transcripts within single cells, but the RNA must still be extracted from the actual cell and processed prior to analysis, which often associates with a loss or damage of the material, as well as the loss of spatial information. Also, all these methods require chemical fixation or lysing and complicated purification procedures to isolate genetic materials, without having the ability to preserve samples after analysis. These destructive methods render no possibility for monitoring single-cell gene expression

different before and after external stimuli, or cell retrieval after analysis, when sample preservations may be needed for further drug response study and guiding therapeutic strategies.

As for CTCs diagnosis, despite various enrichment methods have been developed, due to excessive amounts of accompanying white blood cells (WBCs) in whole blood, the potentially confounding signals from contaminating leukocytes exist with CTCs studies. These WBCs signals in background marginalize CTCs signals in pooled samples; create an issue for downstream molecular analysis [37]. In fact, currently, there is no enrichment method available to get 100% purified CTCs, i.e., contaminating leukocytes are always left behind. In order to address the issue, single cell approaches are explored to enhance sensitivity, often paired with imaging or conventional off-chip methods for gene expression characterization [38-42]. Compared with immunofluorescence assays, accurate measurement of RNA transcripts with PCR-based methods from single cells will enable the precise classification of cell types and characterization of the heterogeneity in cell populations that play critical roles in normal cellular physiology and diseases. The viable release of captured CTC after enrichments is then essential in this case, and it is tough to selectively release and recover single CTCs for downstream analysis with relatively small cell loss [43,44]. Approaches like micropipette aspiration [45,46] and laser microdissection [47] often involve tedious release and pickup process and may be difficult to implement in a clinical setting. A system integrative with current microfluidic enrichment process is needed to utilize the strength of single cell analysis.

1.5 Overview of the single cell analyzer based on nanoprobe platform

To solve these limitations, we developed a sensitive and non-destructive method and apparatus for tracking gene expressions on single cell level within a population of cells, either on a collagen cell culture gel or in a microfluidic environment. For adherent cell lines, the samples are cultured on collagen gel for select-and-probe analysis. An integrated microfluidic/nanoprobe platform is also developed for gene expression analysis of suspension cells on single cell level. This system directly targets and samples down to a few molecules within a single living cell, without the need for purification and averaging typically of conventional technologies. By providing reliable and exceptional sensitivity to identify differences between individual cells in a seemingly homogeneous population, the system creates possibilities for assaying the genomic analysis in living cells and tracking them in response to external stimuli.

1.5.1 Coaxial probe platform for adherence single cell analysis

The single cell analyzer based on nanoprobe platform is developed for analysis of mRNA levels in living single cells. The developed bench-top instrument utilizes a modified AFM (Atomic Force Microscopy) probes for in situ extraction of mRNA molecules from single cells. The modified coaxial AFM probe serves as nanotweezer, and wherein the application of an alternating potential between the inner and outer electrodes of the co-axial cable creates a dielectrophoretic force for attracting target

molecules toward the tip-end. The nanoprobe platform is illustrated in Figure 1.2. An AFM probe that modified with the coaxial feature was positioned over a single cell culturing on collagen gel, and contact with the cell membrane, as well as penetration of the membrane was monitored by changes in the cantilever deflection amplitude. The probe was inserted into the cell for a defined period with the application of AC field for mRNA capture by dielectrophoresis force, the obtained mRNA eluted into solution, and used to prepare cDNA in reverse transcription(RT) process. Transcript levels were determined using qPCR analysis of the samples with significant selectivity and sensitivity. The target cell viability was preserved with low probing voltage for possible further downstream process and study.

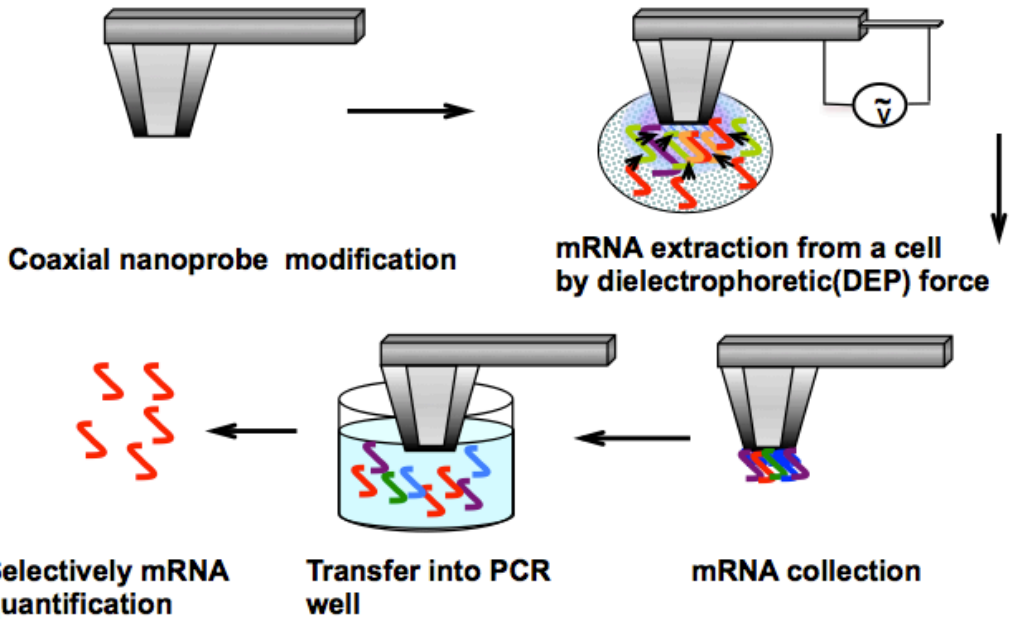

Figure 1.2 Schematic diagram depicting mRNA extraction and quantification using AFM nanotweezers

1.5.2 Nanoprobe/microfluidic platform for gene expression analysis of single cell in suspension

In this work, we have also demonstrated an integrated microfluidic/nanoprobe platform for tracking expression levels of target molecules in a single live cell within a population of cells, in which cells are trapped in an ultra-thin polydimethylsiloxane (PDMS) membrane-sealed chips and form single-cell arrays for probing. It utilizes a modified AFM probes to penetrate through the membrane and extract mRNAs from target cells. The probe is modified to create a tapered coaxial probe as nanotweezer, and wherein the application of an alternating potential between the inner and outer electrodes of the co-axial cable creates a dielectrophoretic force for attracting target molecules toward the tip-end. The extracted mRNA molecules then undergo RT-qPCR process to reveal the single-cellular expression levels of target genes. This trap and probe technique provides no needs of complex cell selectively release process for downstream analysis, renders a perfect approach for single CTCs study with no WBC background contamination. HeLa cell trapping and probing experiments demonstrated cell viability after gene expression analysis, which is the first to facilitate the direct, in situ collection of transcriptional profiles from single cells of interest from a sealed microfluidic device with minimal impact to cell viability.

1.6 Organization of document

Chapter 2 provides detailed descriptions of nanoprobe platform

Chapter 3 discusses in vitro optimizing and calibrating the effect of DEP by using fluorescence microscopy: fabrication, experimental techniques, as well as the theory behind DEP extraction.

Chapter 4 discusses the results from in vivo single cell probing on collagen gel using coaxial probes

Chapter 5 discusses the results from Integrated Microfluidic-AFM platform and its application in single-cell diagnostics for circulation tumor cell (CTC)

Chapter 6 concludes this dissertation with some direction for future work.

CHAPTER 2 DETAILED DESCRIPTION OF NANOPROBE PLATFORM

2.1 Manipulate molecules with DEP force

Dielectrophoresis (DEP) describes the motion of polarizable particles in a non-uniform electric field. The origin of the force lies in differences between the dielectric properties of the particle and the surrounding suspending medium [48]. DEP has been widely used as a method for manipulating and trapping a variety of objects including cells [49, 50], nanoparticles [51], viruses [52], and DNA molecules [53, 54], among which DNA manipulations gain particular attention due to its central role in modern molecular

biology, as well as disease diagnosis, sequence, and forensic investigations [55]. As gel-free techniques to concentrate, trap, size, and separate DNA molecules, most DEP manipulation have been carried out in low conductivity buffers using microarrays and other microelectrode devices.[51,53-55] It is still, however, a challenge to conduct DNA manipulation in biological fluids having high conductivity, e.g. DEP collection of 10nm DNA particles at selected frequency were not able to see in high conductive PBS buffers[56]. It is reported that the buffer conductivity has to be low enough to ensure good performance of DEP [57], sample dilution to low conductance conditions (less than 10 mS/m) was often required before effective DEP separations could be carried out [58], or elution steps have to be performed to re-suspend DNA samples in Hepes-based buffer of smaller conductivity [54]. The limitation of low conductivity environment hinders the application of the DEP technique in physiological conditions, such as DNA separation and concentrating in biological samples.

The magnitude of the dielectrophoresis force acting on the particle depends on the degree of inhomogeneity in the electric field, together with the difference between the dielectric properties of the particle and the suspending medium. It can be shown that the force acting on a spherical particle is given by [48]

$$F_{DEP} = 2\pi\upsilon\varepsilon_m K(\omega)\nabla E^2 \quad (1)$$

where υ is the volume of the particle, E is the RMS value of the electric field (assuming a sinusoidal time dependence), ε_m represents the absolute permittivity of the surrounding medium.

$K(\omega)$ is known as the Clausius–Mossotti (C.M.) factor. It is defined as given by

$$K(\omega) = (\varepsilon^*_p - \varepsilon^*_m) / (\varepsilon^*_p + 2\varepsilon^*_m) \quad (2)$$

In this equation, the complex permittivity of the particle and suspending medium are given as $\varepsilon^* = \varepsilon + j\sigma/\omega$, in which ε is the dielectric constant, σ is the electrical conductivity, ω is the field frequency, and j is the imaginary unit. If $K(\omega)$ is positive, then the particle is attracted to regions of high electric field intensity due to positive DEP. If $K(\omega)$ is negative, then the particle is repelled from regions of high electric field intensity as negative DEP. As the sign of C.M. factor is frequency dependent, experimentally the particles are observed to collect at electrode edges or be repelled away from them, respectively. The value of the applied frequency that results in the cessation of particle motion is defined as crossover frequency. Therefore, measurement of the crossover frequency can be used to characterize the dielectric properties of nanoparticles.

From the expression of C.M. factor, at low frequencies, the DEP behavior of particles is dominated by the conductivity component σ of the complex permittivity. The conductivity of spherical nanoparticle is given by the sum of the bulk conductivity and surface conductivity [50]

$$\sigma_p = \sigma_b + \frac{2K_s}{a} \quad (3)$$

where KS in the general surface conductance, a is particle radius. For polystyrene nanoparticles, the bulk conductivity of is negligible and the particle conductivity is dominated by the movement of charges associated with the particle surface [60].

At high frequencies, the sign of C.M. factor is dominated by permittivity ε difference of particle and medium. The permittivity value depends on the frequency of the applied electric field and can be expressed as [61]

$$\varepsilon(\omega) = \varepsilon_\infty + (\varepsilon_s - \varepsilon_\infty)/(1 + \omega^2\tau^2) \quad (4)$$

Here, ε_∞ stands for the permittivity at frequencies that are high enough that the polarization mechanism cannot follow the changes of the electric field. At very low frequencies, the polarization takes place completely, characterized by static dielectric constant ε_s. The relaxation time τ denotes the time in which the polarization builds up at the characteristic frequency $f_c = (2\pi\tau)^{-1}$.

2.2 Introduction of RT-qPCR for quantitative mRNA analysis

Real-time reverse transcription polymerase chain reaction (RT-qPCR) has become the method of choice for gene expression assessments because it requires relatively little biological material and is efficient. In this method, RNA is first transcribed into complementary DNA (cDNA) by reverse transcriptase from total RNA or messenger RNA (mRNA). The cDNA is then used as the template for the qPCR reaction to quantitatively measure the amplification of DNA using fluorescent dyes. RT-qPCR can be performed in a one-step or a two-step assay. One-step assays combine reverse transcription and PCR in a single tube and buffer, using a reverse transcriptase along with a DNA polymerase. One-step RT-qPCR only utilizes sequence-specific primers. In two-step assays, the reverse transcription and PCR steps are performed in separate tubes, with different

optimized buffers, reaction conditions, and priming strategies. The RT-PCR technique has inherent errors due to variations in technical handling such as pipetting and mixing, as well as different reverse transcription efficiency from run to run. In order to test the degree of variations in our two-step RT-PCR process for single cell analysis, thirty RT-PCR reactions were performed on different days, starting from standard mRNA extraction of 1000 cells stored in an Eppendorf tube at -80 °C. The histogram of obtained Ct value is plotted in Figure 2.1. Starting from the same amount of RNA materials in the tube, the average Ct value of 30 RT-PCR reactions was 17.5275 with a standard deviation (SD) of 0.2630536. The SD of our RT-PCR process was similar as commonly reported. Thus one could expect that for the variations of RT-PCR results from single cell probing, the error of about one cycle could be due to inherent error in RT-PCR steps.

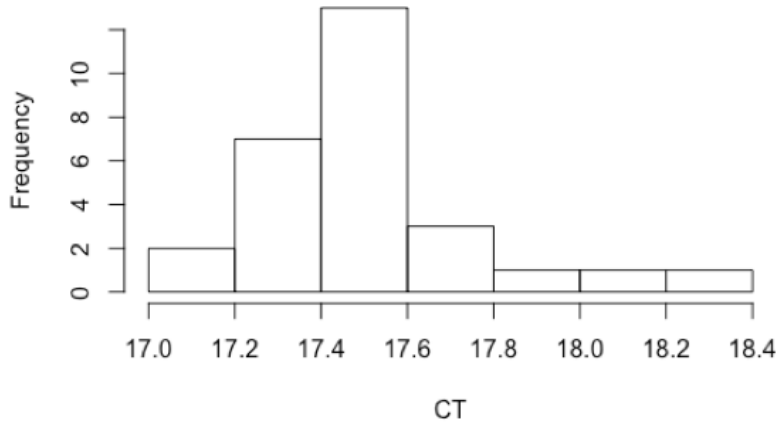

Figure 2.1 Histogram of 30 ACTB Ct values from the same amount of mRNA extraction

2.3 Atomic force microscope (AFM) and AFM probe device

As a topography imaging tools with nanometer precision [62,63], atomic force microscope (AFM) is particularly suitable for micro- and nano-manipulations such as dip-pen nanolithography [64], picking and placing nanoparticles [65], single cell isolation [66,67] and electrostatic nanotweezers [68]. By having both an anode and cathode at the probe end, coaxial AFM probes that concentrate an electric field near their tip have been useful for scanning near-field microwave [69] and optical microscopy [70]. When combining dielectrophoresis with coaxial AFM probes, less work has been demonstrated with dielectric beads only for DEP manipulation [71,72]. Different from DEP microarray- and microfluidic-type devices, tip-like DEP devices, where a local DEP force is generated at the tip end, provides a tool for three-dimensional 3D manipulation of dielectric objects, with excellent precision at sub-micrometer scale.

In this work, we demonstrated a coaxial AFM probe device for DEP manipulation of 20nm polystyrene beads and DNA molecules as well as its usage to extracting mRNA molecules from living cells. The AFM probe is modified to create a tapered coaxial probe as nanotweezer, and wherein the application of an alternating potential between the inner and outer electrodes of the co-axial cable creates a dielectrophoretic force for attracting target particles toward the tip-end.

2.4 Coaxial probe fabrication

The probe was fabricated based on commercially available (Aspire conical probes, nanoscience) highly doped (resistivity 4-6 ohm-cm) conical silicon AFM probes (k˜3N/m), or pyramid access probes (ATEC-NC, Nanosensors) with a spring constant of 45N/m. The conical probes were used for fluorescence in vitro measurements and the pyramid access probes, as the position of the tip end could be easily defined under the optical microscope, were used for cell probing experiments. Such AFM co-axial probe devices are shown in Figure 2.2; it consists of a conducting silicon core and an outer conducting shell, with a dielectric SiO_2 layer in between. The fabrication process started by growing a 60 nm thick layer of SiO_2 on the AFM probe using dry oxidation furnace. The SiO_2 layer served to insulate the entire silicon probe including the AFM cantilever electrically. Then a 10-nm-thick chromium adhesion layer followed by a 30-nm-thick gold layer were deposited on top of the SiO_2 layer by ion-beam sputtering to serve as the outer electrode. In the final step, the Au-coated tip was cut by hitting just the tip-end with the edge of Si_3N_4 wafer during AFM scanning, resulting in the exposure of the inner silicon core with a width of about 300 nm. The cutting step of the tip-end could also be done, and maybe more commonly, with focused ion-beam (FIB) cutting [73].

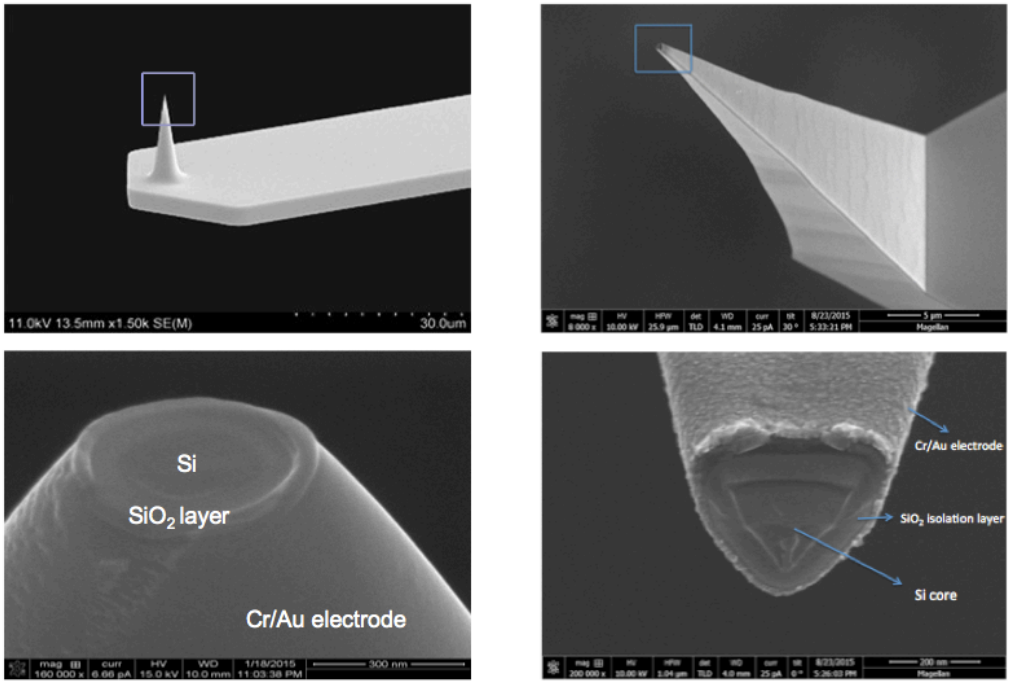

Figure 2.2 Scanning electronic microscopic (SEM) images of the coaxial AFM probes. Left: coaxial pyramid probes fabricated by edge cutting; right: coaxial conical coaxial probes fabricated by FIB

2.5 The setup of nanoprobe platform

Figure 2.3a shows the bench-top hardware set up for the cell on gel probing with full functions of motorized zoom/focus for imaging as well as motorized probe/sample movements. A 10X lens and LED illumination stage were equipped with optical filter slots for fluorescence imaging capability. The optically encoded step motor Z-stage had calculated moving resolution of 10nm, while XY stages had resolutions of 100nm in movement. To maintain cell activity during the probing experiments, which usually last around one hour depending on the number of cell samples, a cell culture stage was designed and fabricated (Figure 2.3b). The idea of cell sample stage was to hydrate

target cells by having cells grown on top of microporous substrate or hydrogel so that the growth media could continually feed cell from underneath the substrate by placing the cell substrate on top of media reservoir. The cell on gel set up will be described in details later in Chapter 4. The stage reservoir had inlet/outlet channels for growth media exchange, and a heater on the side to maintain the stage block at 37 °C. As we have developed releasing method to release the target molecules from the probe into droplets of reverse transcription (RT) buffers, a sample releasing stage was also designed with aluminum pillow array for holding releasing droplets as well as defines the spatial coordinates of each droplet for automating the probing and releasing process.

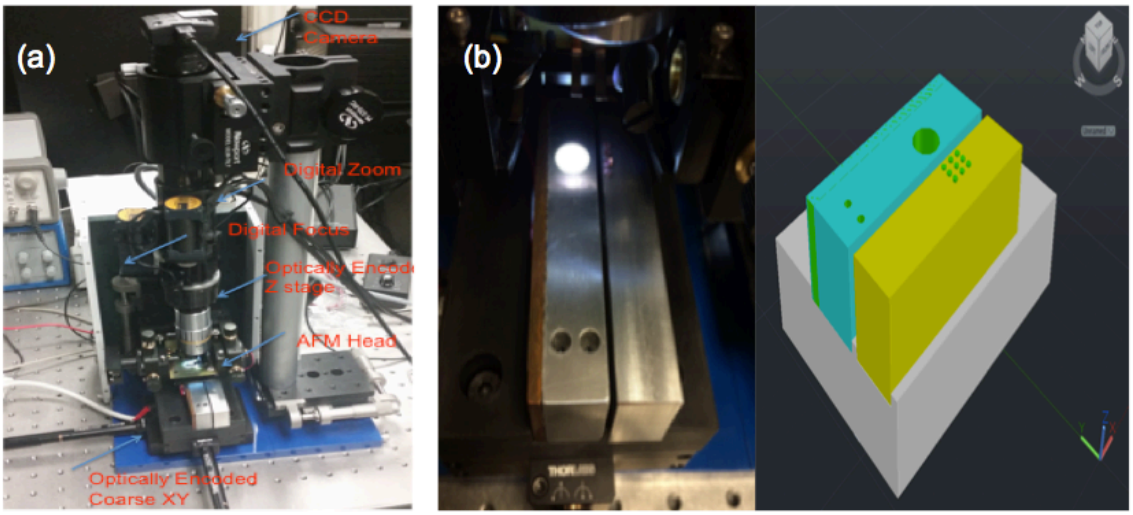

Figure 2.3 (a) instrument set up for cell on gel probing (b) images of cell and sample releasing stages, and CAD drawing of current platform which has cell and sample stages sitting on top of illumination stage

Along with all above hardware developments, control software with graphical user interface was developed using LabVIEW program to semi-automate the probing and releasing process. The XYZ probe/sample stages could move in user defined distance within stage resolutions. By selecting target cell on the camera image, the software could position the tip over a selected cell for probing. Each coordinate of target cells and releasing pallet are registered before probing so that the probe can be moved back and force between the target cell and releasing droplets for multiple sampling. Base on the new platform, the sampling throughputs was increased.

Another setup of integrated nanoprobe/microfluidic platform for single cell analysis in microfluidic chips is shown in Figure 2.4. The system was setup on top of an inverted microscope. The system has an adapting stage for holding microfluidic chip, as well as fully digital control of image zooming/focusing, samples positioning, and penetration. As the platform was setup on top of an inverted microscope, it could also be used for high magnitude imaging associated with cell probing as well as fluorescence measurement at the probe end such as described in Chapter 3. The LabVIEW controlled graphic user interface was also developed for this platform to facilitate operation.

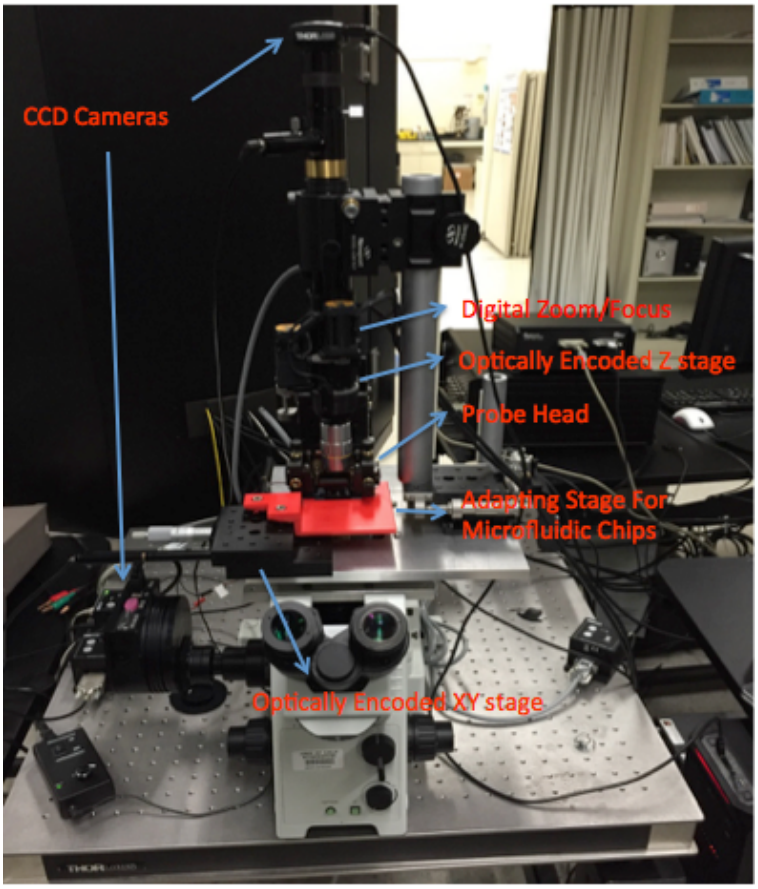

Figure 2.4 Integrated nanoprobe/microfluidic platform for single cell on top of X71 Olympus microscope

CHAPTER 3 OPTIMIZE AND CALIBRATE THE EFFECT OF DEP IN VITRO BY USING FLUORESCENCE MICROSCOPY

In this chapter, we demonstrated the coaxial AFM probe device for DEP manipulation of 20nm polystyrene beads and DNA molecules. The AFM probe was modified to create a tapered coaxial probe as nanotweezer, and wherein the application of an alternating potential between the inner and outer electrodes of the co-axial cable created a dielectrophoretic force for attracting target particles toward the tip-end. The DEP performance of coaxial probe device was investigated in both low and high conductivity buffer conditions with the positive DEP collection of the nanoparticles in the high-field regions. Unitizing the high electric fields generated by the application of modest voltages without electrochemical effect, working condition for positive DEP trapping of DNA molecules were successfully extended to high conductive buffers (larger than 100mS/m). The frequency response of DEP manipulation of dielectric objects using coaxial AFM DEP tweezers was investigated, for the first time, over a high-frequency range from 100KHz to 50MHz.

3.1 Fluorescence measurement in low conductive buffer condition

The effect of DEP was first characterized in vitro under a fluorescent microscope using dye-labeled double-stranded DNA molecules. 2.7kb pUC 19 plasmid DNA (Thermo Scientific) was labeled with yoyo-1 dye (Thermo Scientific)

at approximately one yoyo-1 molecule per 10 basepairs. AlexoFluor488 filter set was used for these experiments. Coaxial probes were mounted on a holder with separated electrical contacts for the inner silicon electrode and the outer ground metal shield. The probes were immersed into nanoparticle suspension on top of glass cover sides, with all the electrical contacting parts remaining in the air. Movement of the molecules was observed using Olympus IX71 inverted microscope equipped with motorized translation stages (Thorlabs). An oil-immersion objective 100X was used, together with cooled CCD Camera (Photometrics) for recording images. The voltage across the coaxial probe was applied using a Hewlett Packard function generator with the frequency range up to 50MHz.

The DNA molecules were diluted to a concentration of 1.2ng/μl in 0.1X TE buffer with a conductivity of 6mS/m. This is a typical working condition for DEP particle manipulation in solutions with low conductivity (less than 10mS/m) [51,53,54]. The DEP effect on these molecules is demonstrated in Figure 3.1, where a time series of images shows DNA accumulating in between the inner silicon core and the outer gold electrode of coaxial probes; when a 1.5 V_{RMS} AC voltage at 10MHz was applied to our co-axial AFM probe. Following the application of the AC field, the DNA molecules started to accumulate on the probe end and gradually formed a fluorescence ring structure after 60s. Figure 3.2 showed normalized fluorescence intensity at the probe end as a function of time after applying AC voltage. The fluorescence pattern and signal strength increased as a function of time indicating the DNA molecules accumulated at the probe end due to positive DEP force. The

fluorescence intensity did not change further with prolonged AC field application after applying AC voltage for 60s.

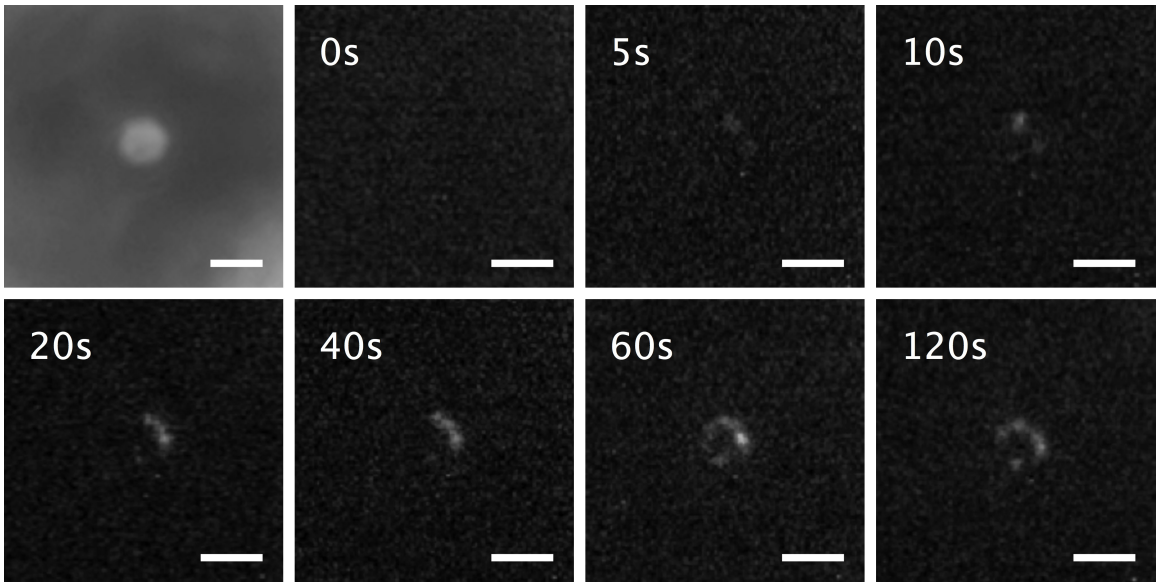

Figure 3.1 Bright field image and time series fluorescence images of yoyo-1 dye labeled DNA focusing on the probe end in 0.1X TE solution with the application of 1.5 VRMS AC field at 10MHz, scale bar: 1.5 μm

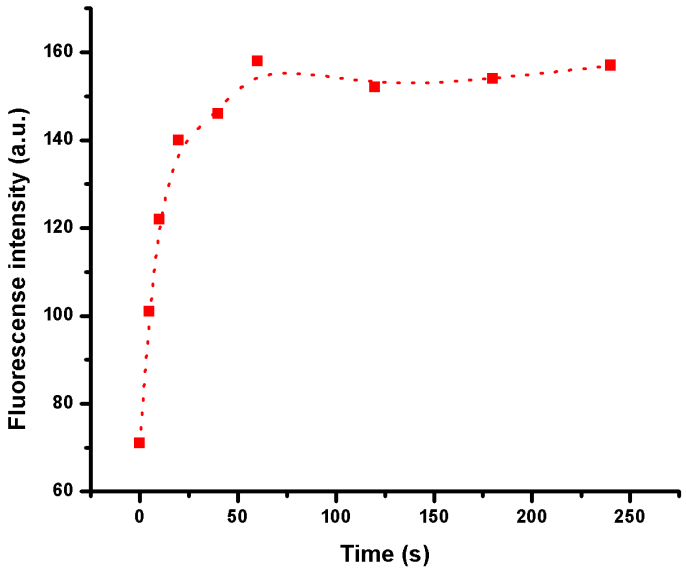

Figure 3.2 Normalized fluorescence intensity at the probe end as a function of time after applying AC voltage

3.2 Field intensity simulations of coaxial nanoprobe

The 3D distribution of electric field strength at the probe-end for the DEP attractive force was calculated by the finite element method (FEM) solver (COMSOL Multiphysics). When a 5 Vpp, 10 MHz AC field was applied between the Si core and Cr/Au outer electrode, the calculated electric field at the probe-end was in the range of 10^8V/m (Figure 3.3). The largest electric field distributed in the oxide part in between inner core and the outer electrode with clear a ring pattern. The ring structure agrees well with our simulation results where the highest field intensity occurs in the ring region in between inner and outer electrodes; the DNA molecules accumulated at the probe end due to positive DEP force.

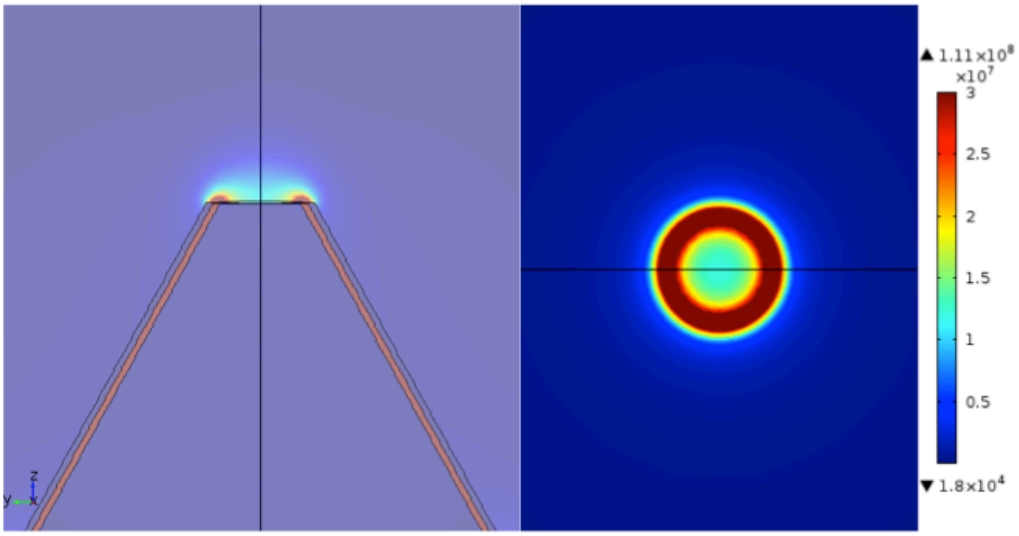

Figure 3.3 Finite element electrostatic simulation of electric field of a coaxial probe

3.3 Fluorescence measurement under high conductive buffer conditions

3.3.1 Fluorescence measurement with polystyrene nanoparticles

To investigate the performance of DEP tapping with our coaxial probe device under high conductivity buffer conditions, we tested the probe with 20nm polystyrene beads of known dielectric properties [52,74]. The polystyrene beads used for DEP experiments were 20 nm diameter carboxyl-modified FluoSpheres® (Invitrogen) with yellow emission at the wavelength of 575 nm. The 20 nm diameter polystyrene beads were supplied as 2% solids (w/w) in aqueous solution (2 mM sodium azide in distilled water). The stock solution was diluted 10^5 times with DI water. For high conductive buffer experiments, a same fold of dilution was made with 0.1X PBS buffer. TAMRA filter set was used for imaging fluorescent polystyrene beads. The probes were immersed into nanoparticle suspension on top of glass

cover sides, with all the electrical contacting parts remaining in the air. An oil-immersion objective 100X was used, together with cooled CCD Camera for recording images.

Figure 3.4A-C shows the collection of 20 nm fluorescent beads with positive DEP force in DI water with the application of AC voltage at different frequencies. The images were obtained 30 s after voltage application, with the camera gain and exposure settings kept constant. It was found that with the same field application time and drive voltage, the polystyrene beads had higher collection rate at the low-frequency range. Particles concentrated on the probe end immediately diffused away after turning off the AC field, as indicated by the absence of fluorescence at the probe end. The off time between measurements at different frequencies was approximately 10 s, long enough for the system to recover before each DEP field application. The fluorescence signal intensity at probe end was determined over frequencies from 200KHz to 50MHz after subtracting the fluorescence background. The fitting of our experimental data to the Clausius–Mossotti model is plotted in Fig. 3D, using $\varepsilon = 2.5$ for polystyrene nanoparticle, $\varepsilon = 78$ for medium permittivity and 2mS/m for medium conductivity. Fluorescence signal onset frequency was around 6MHz for our coaxial probe device. If we assume that the zero-force point or crossover frequency to be approximately 6MHz, then solving $\sigma_p = \sigma_b + 2K_s/a$ with $\sigma_b = 0$ yields a particle surface conductance of 0.48nS, close to the reported value for particles of similar particle size [52]. This value is also consistent with values for larger size particles since smaller nanoparticles normally have lower

surface conductance [75]. DEP bead collection tests were also performed in high conductivity buffer conditions. Within the frequency range from 100KHz to 25MHz, no fluorescence signal change was observed at the probe end while applying the AC field in 0.1X PBS buffer. This indicates that conditions for positive DEP force are not satisfied for this case. When the dielectric constant of the particle is smaller than that of the surrounding medium, and in a high conductivity buffer medium where the conductivity is higher than that of the particles, a negative C.M. factor is obtained, as plotted in Figure 3.4D.

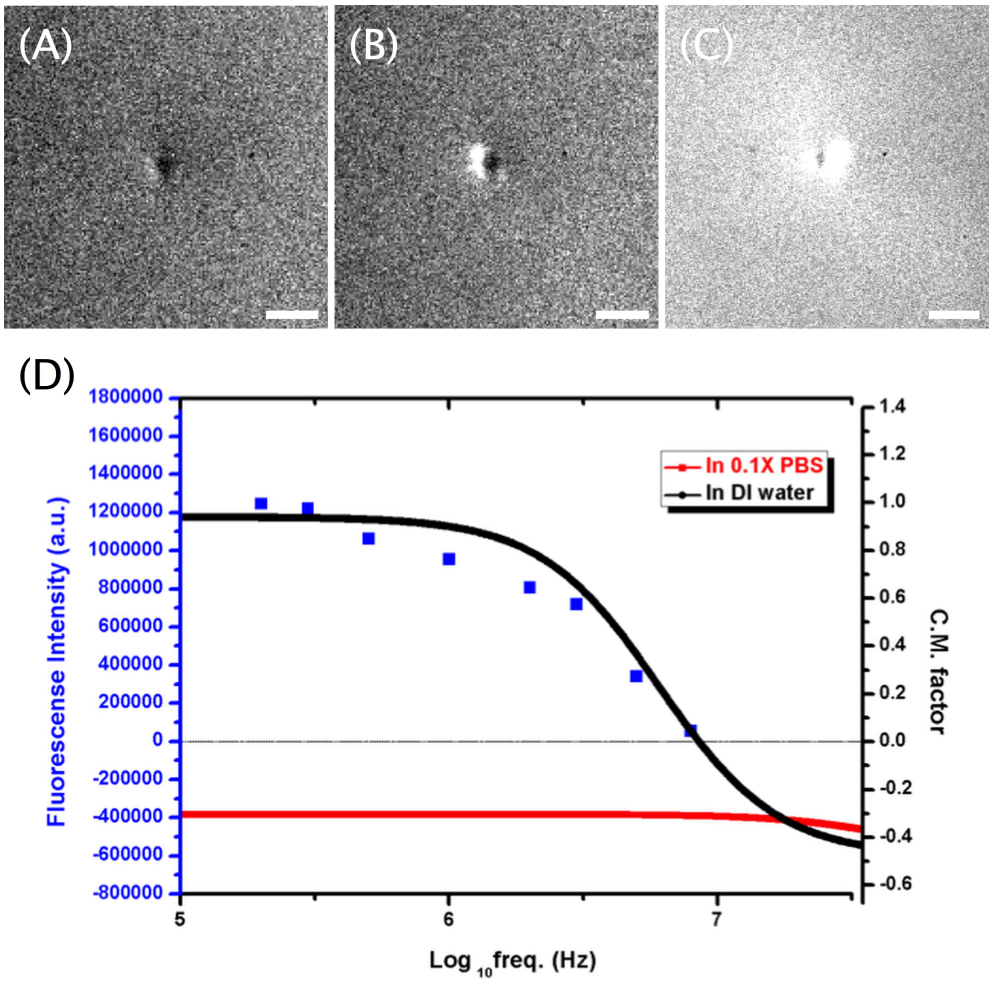

Figure 3.4 Fluorescence microscope pictures of 20nm polystyrene nanoparticles accumulating at the probe end in DI water at different applied frequencies with a voltage of 2VRMS, scale bar: 1.5 μm. (A) Before applying voltage (B) Applying voltage at 5MHz for 30s (C) Applying voltage at 200KHz for 30s (D) The fluorescence signal intensity of polystyrene nanoparticles at probe end after 30s of DEP collection with field frequency from 200KHz to 50MHz. Solid curves correspond to the Clausius–Mossotti model in DI water and 0.1X PBS with conductivity of 2mS/m and 160mS/m, respectively

3.3.2 Fluorescence measurement and analysis with dye-labeled DNA

DEP focusing of DNA molecules using our probe device was tested under high conductive buffer condition in 0.1X PBS. As shown in Figure 3.5, with the application of AC voltage at 1.5 V_{RMS} at 10MHz, the DNA molecules started to accumulate on the probe end. The fluorescence signal increased as a function of time and gradually formed a ring structure within 1 minute, similar to the situation when in low conductivity buffers. Our data showed that DNA molecules concentrated on the probe end due to positive DEP force at applied AC field conditions in high conductivity buffer - different from microelectrode DEP devices where one has to rely on low conducive buffers for DNA manipulation[50,57]. It should be pointed out that in this set of experiments we used DNA concentrations (12ng/μl) that were ten times higher than those used for low conductivity buffer environments, to get clear fluorescence signals for demonstration.

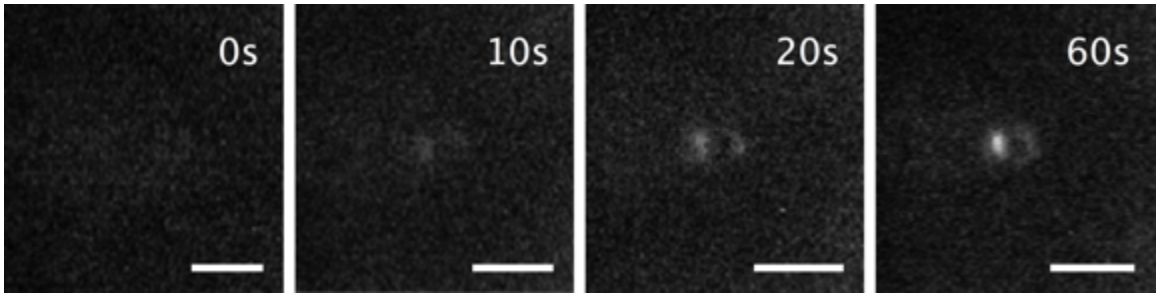

Figure 3.5 Fluorescence images of yoyo-1 dye labeled DNA focusing on the probe end in 0.1X PBS buffer with the application of 1.5 VRMS AC field at 10MHz, scale bar: 2 μm

3.4 The effect of AC frequency on the capture efficiency of DEP coaxial probe

Similar to the nanoparticle experiments, the fluorescence signal intensity of DNA molecules at probe end was collected over frequencies from 100KHz to 50MHz after applying field for 60s at each frequency. At high frequencies, the sign of C.M. factor is dominated by permittivity ε difference of particle and medium. Here the permittivity of DNA molecules is calculated using equation 4 (Figure 3.6) using values for the infinite frequency dielectric constant ε_∞ = 78, static dielectric constant ε_s =118, and characteristic frequency $f_c = (2\pi\tau)^{-1}$of 9MHz [61,76]. The permittivity of DNA decreases with increasing frequency. The aqueous medium permittivity is chosen to be constant at 78, as it does not vary much with frequency or salinity change [77].

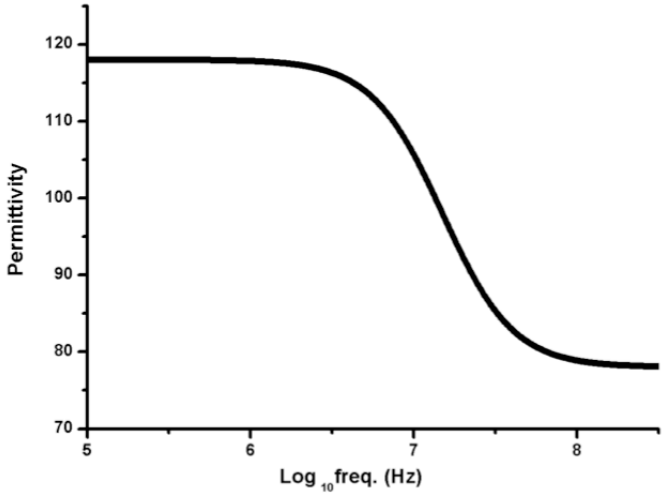

Figure 3.6 the permittivity of DNA molecules as a function of frequency

Since the holding piece of our AFM probe cantilever device consists of an inner silicon and insulating layer and an outer metal electrode, it acts as a planar capacitor with a characteristic cutoff frequency, the AC voltage applied to the holding piece will not transmit its signals all the way to the co-axial probe end of the cantilever beyond a particular cutoff frequency (Figure 3.8 black curve). We measured the impedance of coaxial probe device over 100KHz to 50MHz range using an impedance analyzer (Agilent). The RC circuit model (Figure 3.7B) was used as equivalent circuit model of our probe device and indicated an equivalent resistance of $75.3255\,\Omega$, inductance of 427.717nH and capacitance of 188.089pF. The impedance value calculated based on the RC circuit model fit well with measurement as shown in Figure 3.7A. Cut off frequency of RC circuit was calculated using $fc = 1/2\pi RC$, indicated a cutoff frequency of around 12MHz.

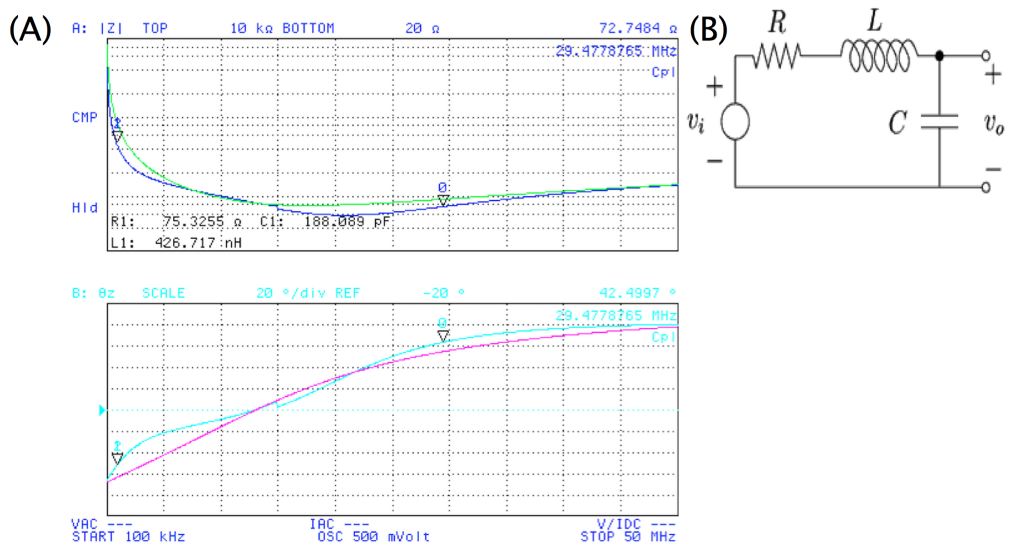

Figure 3.7 Impedance of coaxial probe device over 100KHz to 50MHz. (A) dark and light blue curves correspond to measured |Z| - θ values, green and pink curves correspond calculated |Z| - θ values based on circuit model in (B)

Corrected values of C.M factor after factoring in this frequency cutoff is shown in Figure 3.8(green curve). Due to the capacitive cutoff effect of our probe device, no fluorescent focusing effect was observed when the AC voltage frequency was above 25MHz even though this is still within the working frequency range from the Clausius–Mossotti model. Fitting of the experimental data below cutoff frequency to the C.M. model indicates a surface conductance of 3.95nS for DNA molecules - within the range of previously reported values [78], if one assumes a particle size of 50nm [79].

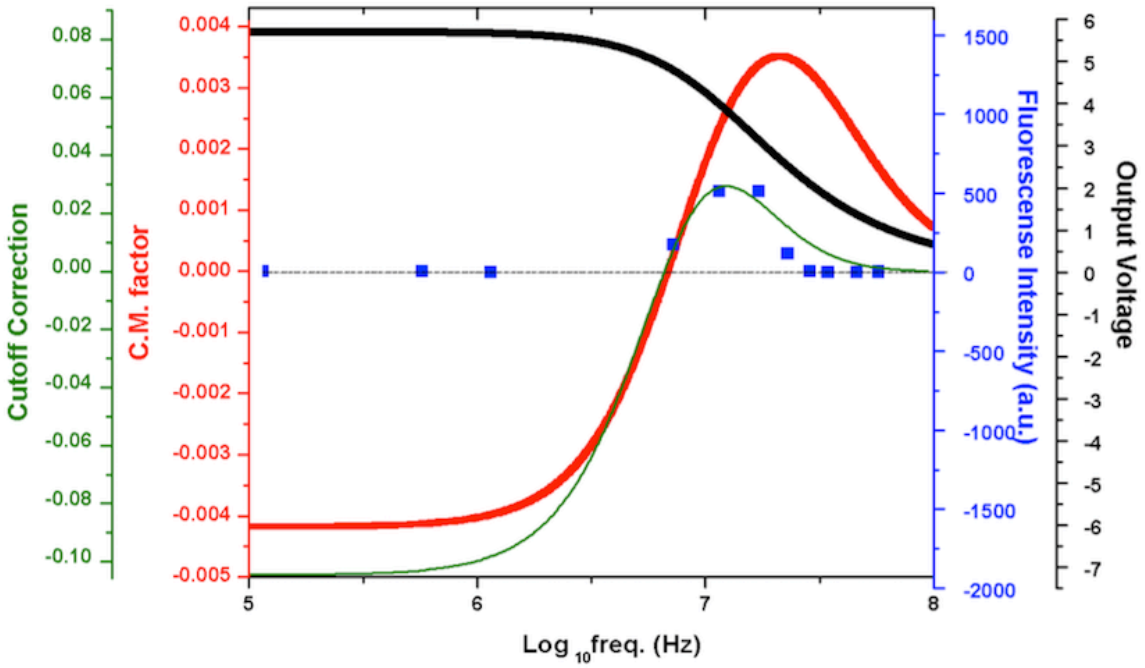

Figure 3.8 Blue dots: fluorescence intensity of DNA molecules focused at probe end in 0.1X PBS over frequencies from 100KHz to 50MHz after applying field for 60s at each frequency; Red curve: Clausius–Mossotti model for DNA molecules in 0.1X PBS with conductivity of 160mS/m; Black curve: output voltage of coaxial probe device calculated from RC low pass model if 5Vpp input voltage is applied, the RC values were obtained from probe impedance measurement. Green curve: corrected values of C.M model after considering RC frequency cutoff. The curve was obtained by multiplying values of C.M. factor (red curve) with square of output voltage values (black curve)

3.5 The effect of buffer conductivity

3.5.1 Finite Element Model simulation

As it was needed to increase DNA concentration, compared with low conductivity environment, to observe DEP effects in PBS buffer. Investigates were carried out to find out why there is weaker or no DEP effect found in high conductivity buffers based on fluorescence measurements, and possibly why many conventional DEP devices have to use low conductive solution as essential working conditions. Simulations of electrical field intensity at probe end indicated that the field intensity decreased to half of its original value when increasing the conductivity of the surrounding medium from 0.01S/m to 0.49S/m (Figure 3.9), as from the screening effect of higher concentration ions at probe end.

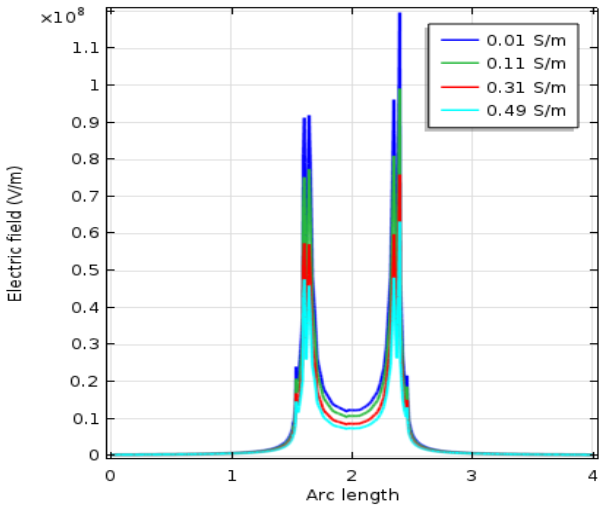

Figure 3.9 Line plot of field distribution at the probe end in mediums with different conductivity from 0.01S/m to 0.49S/m

3.5.2 Fluorescence measurement and analysis

The fluorescence emission spectrum of dye labeled DNA indicated that the fluorescence intensity decreased with respect to the increasing of ion concentrations(Figure 3.10).This is due to fluorescence quenching in the presence of salt ions[80,81].

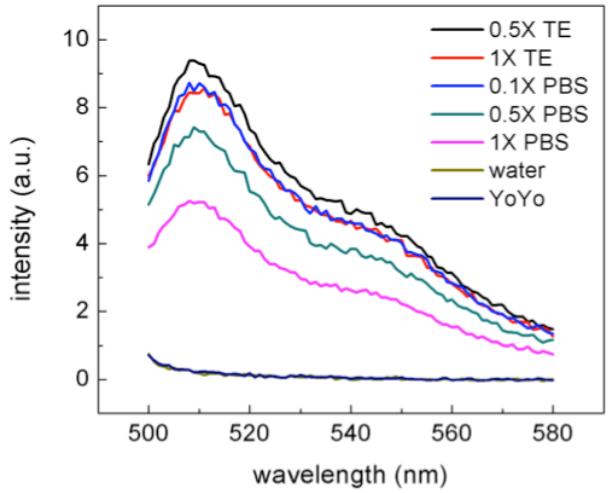

Figure 3.10 Fluorescence emission spectrum of yoyo-1 labeled DNA in different buffers

3.5.3 C.M factor analysis

As already shown for the case of DEP nanoparticle focusing, the values of the C.M. factor changed in high conductive medium. Based on the frequency dependent permittivity values, the C.M factor for DNA molecules in both DI water and 0.1X PBS were plotted as a function of frequency (Figure 3.11). Here the values in 0.1X PBS were multiplied by 100 to plot data on the same scale as those for the low conductive medium condition. The difference of positive C.M. values between these two cases indicates that low conductive medium is the preferred working condition

for DNA DEP manipulation, where the value of C.M. factor decreased with increasing frequency in the megahertz range, as experimentally observed by others [54,55,82]. DNA molecules in solution have a compensating cloud of counterions that are readily polarized by an electric field [83]. The permittivity of DNA is higher than the surrounding medium - different from the case of polystyrene nanoparticles. Thus at high frequency when permittivity term dominates, the values of C.M. factor become positive in high conductive medium condition, as indicated by our experimental results, although the value is much smaller than when in a low conductive environment. The lower value of C.M. factor, together with screening and quenching effects of salt ions, contribute negatively to particle concentrating by DEP effect, make it hard to either achieve or observe DEP manipulation of DNA molecules in high conductive medium, addition to possible electrochemical effect associated with increased buffer conductivity.

Compared with DEP devices based on microelectrodes, the coaxial probe device, utilizing the nano-scale separation between the inner and outer electrodes, could easily achieve a field intensity of 10^8 V/m when a low voltage of $1.5V_{RMS}$ is applied; The scaling effect has also been demonstrated with microelectrode DEP device where one gets a stronger force by scaling down the characteristic length of the system while keeping the voltage constant . This field strength of coaxial probe device, however, is of magnitude higher than reported conventional DEP device for in vitro molecule manipulation [56]. This is the reason our probe device has successfully achieved positive DEP trapping of DNA molecules in a high conductive

buffer condition where others have failed. The applied voltage at high frequency also eliminates electrochemical effects; we saw no bubbling events when applying voltages at frequencies greater than 100KHz in high conductive buffers.

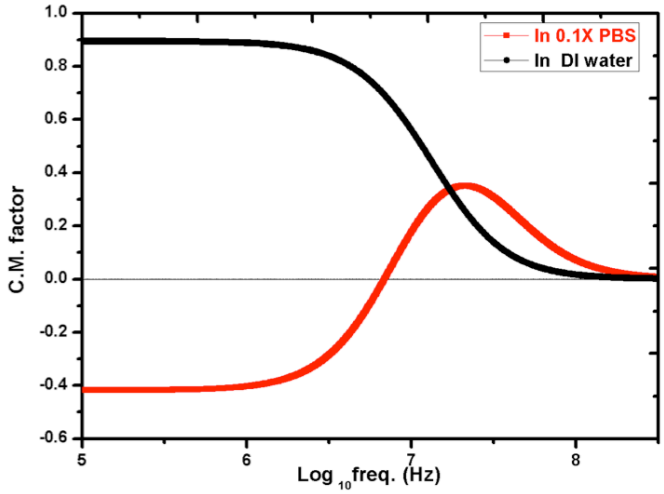

Figure 3.11 Clausius–Mossotti model of DNA molecules in DI water and 0.1X PBS with conductivity of 2mS/m and 160mS/m, respectively. The values in 0.1X PBS were multiplied by 100 times to plot on the same scale

3.6 Summary

The application of coaxial AFM probes in a novel tip-like DEP device for polystyrene nanoparticle and DNA molecules manipulation and trapping in both low conductive (6mS/m) and high conductive (160mS/m) buffers were demonstrated. The 20nm nanoparticles concentrated on the high field region at the probe end due to positive DEP force in low conducive solution environment and experienced

negative DEP force in high conductive buffer condition. Positive DEP trapping of DNA molecules in low conductive solutions has been reported. We have not only demonstrated nanoscale trapping of DNA molecules using positive DEP in low conductive solutions but have also shown that the ultra high field generated at the co-axial AFM nanoprobe end can be used to create a positive DEP and successfully concentrate DNA molecules in high conductive buffer. The effect of DEP focusing was quantified using fluorescence and compared with classical Clausius–Mossotti theory. Our experiments have also been able to estimate the effective permittivity and surface conductance of nanoparticles. Earlier work using DEP microelectrode devices were limited to two-dimensional manipulations. The coaxial DEP probe is a new a tool for three-dimensional manipulation of dielectric objects in medium, with fine precisions at nanometer scale like conventional AFM probes. The ability to work in high conductive buffer environment with DNA molecules is critical for the application of DEP to biomedical research.

CHAPTER 4 IN VIVO SINGLE CELL PROBING USING COAXIAL NANPROBLES

4.1 Experimental procedure

The fabricated coaxial probes were tested for single cell probing in vivo. Human Hela cells were used in this set of experiments by culturing cells on top of substrates. HeLa cells were cultured in DMEM medium (Gibco) supplemented with 10% fetal bovine serum (FBS; Gibco) and 1% penicillin/streptomycin (1000 U/mL, Gibco). Cells were passaged every 3-4 days following standard protocols and cultured in a humidified incubator at 37 °C with 5% CO_2. The cells were seeded on substrates after passaging and waited for at least two days before probing.

RNA expression experiments were performed by inserting into the cytoplasm region around the nucleus to collect mRNA. The AFM tip was positioned above a target cell under an optical microscope with digital zoom/focus function. The coaxial probe approached the cell surface by giving the command to step motorized translation stage, where the coaxial probe holder was attached. The touch of the tip on the cell surface was detected by the deflection signal of the probe cantilever. Once contact was established, a short voltage pulse was applied to the z-piezo on the probe holder to penetrate the cell membrane. The penetration processes were monitored by running force/distance curves in contact mode using an atomic force microscope (MPF-3D, Asylum) as shown in Figure 4.1. For each probing, there was a small glitch on the

approaching line (red curve) of force/distance curve, indicating the penetration of cell membrane. While for the control sample where the probe touched substrate only without probing cell gave a regular linear increasing of force signal with no glitch spot on the curve. Also, for cell probing curves there were bigger separations between approaching (red) and retracting (blue) curve, the penetrations occurred closely to the point where probe/cell contacts were established. Using the established probing procedure, it was easy for the coaxial probe devices to penetrate cell membrane for mRNA collections. Once the probe was inserted into the cell, 10MHz voltage at $1.5V_{RMS}$ was applied across the inner and outer electrodes of the coaxial probe device. After 90 s, the probe was removed from the cell with AC voltage still be on.

After single-cell mRNA probing, the extracted mRNA molecules were released from the probe end into PCR tubes containing reverse transcriptase assays. Reverse transcription was carried out to generate complementary DNAs (cDNAs) using the iScript™ cDNA Synthesis Kit (Bio-Rad). Thereafter, for the qPCR analysis of each target gene, 10% of the total cDNA product from a single cell was transferred into a PCR tube as suggested in the manufacturer's protocol. For real-time qPCR cycling, SYBR® Green (Bioline) was used as the reporter dye in the Chromo4 qPCR instrument (Bio-Rad). The following thermal cycling protocol was used: 45 cycles of 94 °C for 10 s, 59 °C for 10 s and 72 °C for 20 s. The melting curves were generated by increasing the temperature from 60 °C to 95 °C and holding for 10 s after each 0.2 °C temperature increment. As for the positive controls, mRNAs extracted from bulk cell lysates using cell-lysing RNA

extraction kit (ISOLATE II RNA Mini Kit, Bioline) were diluted to a concentration of 10 cells' mRNA molecules per 5 µL distilled water, and were quantified following the same RT-qPCR process as mentioned above.

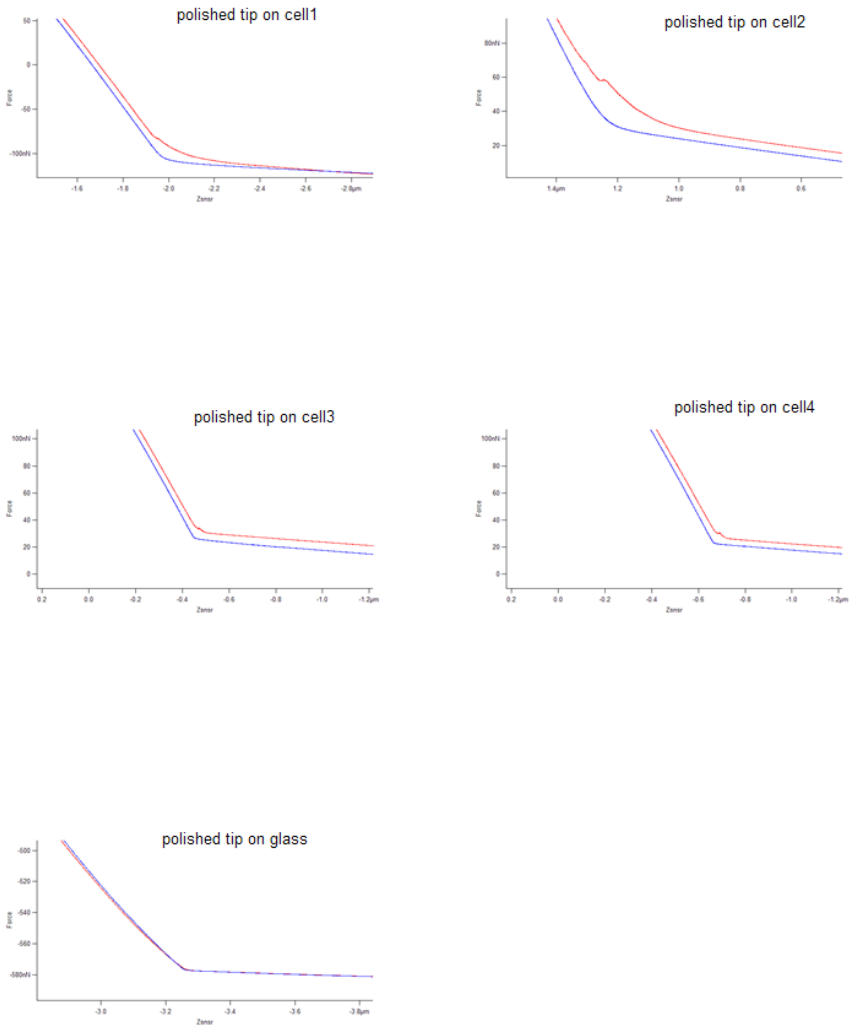

Figure 4.1 Force-distance curves of cell probing processes using coaxial probes

4.2 Cell on gel setup for background elimination

The probing experiments were first performed using cells growing on glass substrates (Figure 4.2). The gene expression level of each cell was studied by looking into the expressions of three housekeeping genes under the applied AC field of 1.5 V_{RMS}, 10 MHz: ACTB (beta-actin), a high-abundant gene; GAPDH(glyceraldehyde 3-phosphate dehydrogenase), a medium-abundant gene; and HPRT(hypoxanthine

phosphoribosyltransferase), a low-expression gene (<10^2 copies per cell). However, aside from getting positive PCR readings from probes that inserted into target cells, we also got readings from probe devices that touched growth media only, yet without actually probing cells. The readings of ACTB and GAPDH for both sets of samples were close to each as shown in Figure 4.2b. This indicated that we had background readings from cell culture media and the PCR readings we got from cell probes were the false positive signal. Later we figured out that the background reading in cell culture media was from floating cell debris or detached dead cells that stick on the coaxial probes during cell probing. These cells/cell debris also got transferred into following RT-PCR process for reading out. As we were doing single cell mRNA measurements where the positive signals from extracted mRNA molecules were so low (less that 5pg), a single detach cell sticking on the probe device could provide false signal burying the actually reading from the target cell. To solve this problem of background problem in cell culture medium, several methods were tested, including utilizing hydrophobic coatings on the probe surface to prevent the amount of cell culturing medium as well as its content sticking on the probe device during probing, or coating the glass substrates with ECM to increase cell attachment and decreasing cell culture density on substrate as well. Combining these methods helped in reducing background reading from the medium, yet sometimes it was not able to obtain a clean background that was less than the reading from target cells, especially when interested in getting copy numbers of genes with relatively low expression levels such as HPRT (<10^2 copies per cell).

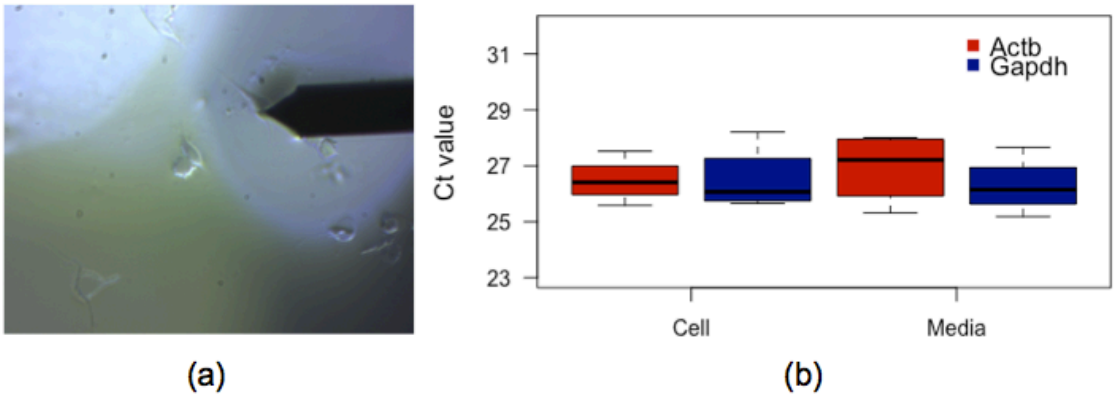

Figure 4.2 (a) Probing cells culturing on glass substrates. (b) The averaged Ct values of ACTB and GAPDH from probes probing target cells and from probing culture media only

Consequently, a new cell on gel setup was developed where cells were cultured on collagen gel (Advanced BioMatrix) for probing as shown in Figure 4.3. The substrate used was porous polycarbonate membranes with pore size of 3~5µm. Then collagen gel with a thickness of 1~2mm was prepared on top of polycarbonate membranes by incubating inside cell incubator for 1 hour. After gels had been totally solidified, Hela cells were seeded on the gel and cultured in cell culture dish for two days before probing. The gel substrates were placed on top of homemade sample stage with media reservoir as described in Chapter 2 during cell probing. Due to the microporous feature of polycarbonate membranes as well as collagen gel, the growth media could continually hydrate and feed cells from underneath. While the top surfaces of target

cells were exposed for probing in air, this setup eliminated the risk of having probe device in contact with cell culture media and giving background readings consequently.

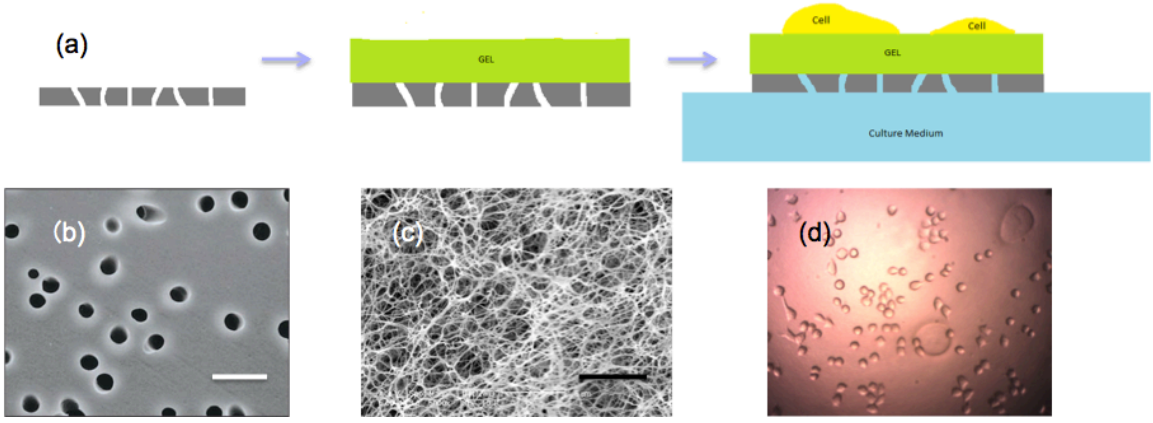

Figure 4.3 (a) Illustrating of the cell on gel setup for single cell probing. (b) SEM picture of polycarbonate membrane, scale bar: 10μm. (c) SEM image of collagen gel, scale bar: 5μm. (d) Optical image of Hela cell growing on top of gel surface for probing

The bright-field microscopic image of single-cell mRNA extraction using the coaxial AFM tip is shown in Figure 4.4a. The was no obvious changing in cell morphology before and after probing. RT-qPCR results of mRNA probing from single Hela cells on collagen gel are shown in Figure 4.3b to demonstrate the feasibility of the assay. The mRNA molecules isolated from 10 Hela cells by cell lysing mRNA extraction kit (pink line) was used as a reference, and had a Ct value of 23.50 for ACTB. The Ct values of ACTB mRNA molecules extracted by AFM probing from two different Hela cells at AC field strength of $1.5V_{RMS}$ were 29.18 and 29.23. The Ct values of GAPDH mRNA molecules were 28.63 and 28.90, the Ct values of HPRT mRNA molecules were 32.16 and 32.96 respectively. The readings from probing gel only but did not go inside cell showed negative readings

with no PCR amplification, indicating that there was no background reading now by preventing contaminations from cell culture medium using the cell on gel setup. The results showed that target mRNAs were successfully picked up with the application of AC field. Gene expression analysis with different PCR primers indicated that multiple transcripts, including ACTB and GAPDH with high abundance, as well as HPRT with low copy numbers could be studied from one probing result.

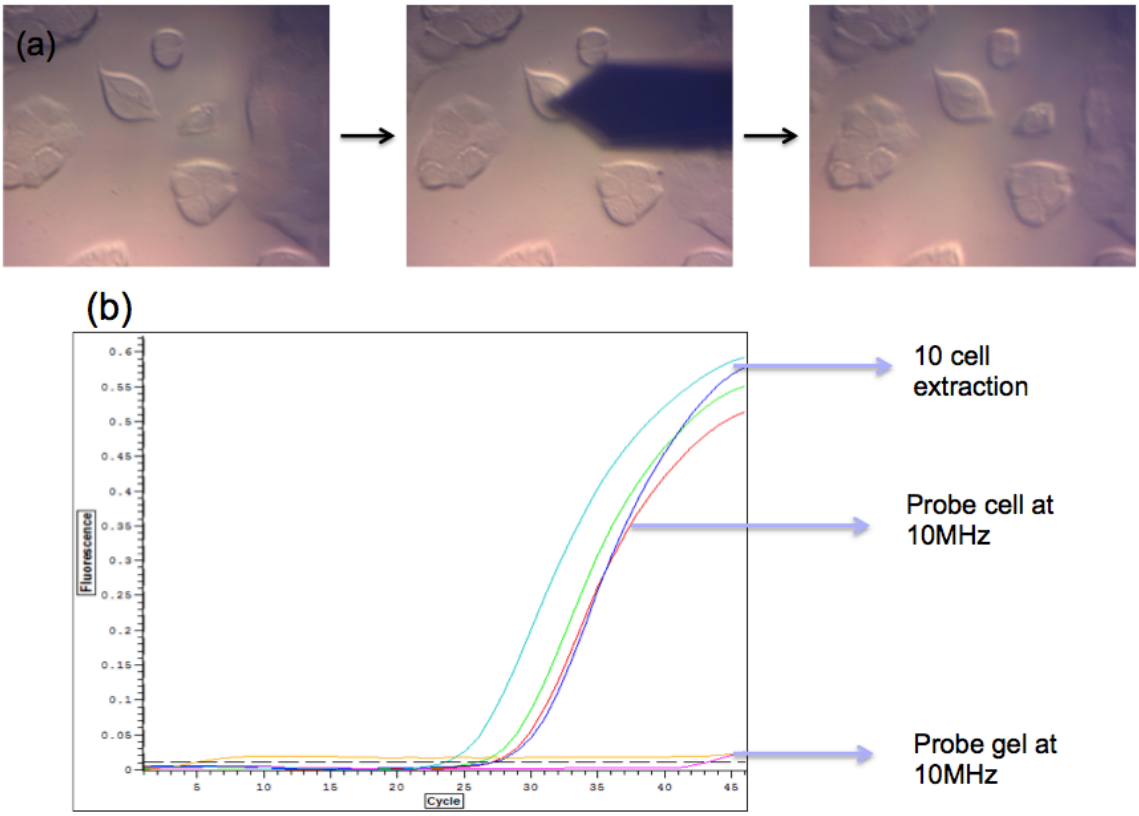

Figure 4.4 (a) Optical images of single-cell mRNA extraction process using the coaxial probe. (b) RT-qPCR results of mRNA probing from single Hela cells on collagen gel

4.3 Standard curves generation for quantitative analysis

To quantify the mRNA extracted from single cells using our experimental techniques with qPCR quantification, a serious of standard curves were generated by using synthetic DNA templates with known concentrations (IDT DNA). The DNA templates had the same sequence as RT-PCR amplicons when for mRNA RT-qPCR. In qPCR, the standard curve is a plot of the logarithm of concentration vs. the threshold cycle, which is a straight line with a negative slope as shown in Figure 4.5. For curve generation, ten-fold dilutions of stock DNA templates were prepared with ultrapure water. Then the known numbers of template molecules were pipetted into PCR wells with at least three replicates for each sample dilution. In this way the Ct values from PCR and copy numbers of DNA templates in each PCR reaction well were associated, the standard curves were generated by plotting of the logarithm of the number of molecules vs. the threshold cycle as Ct values, which is a straight line with a negative slope as shown in Figure. 4.5. These curves were then used for interpreting mRNA extraction readings from single cell probing.

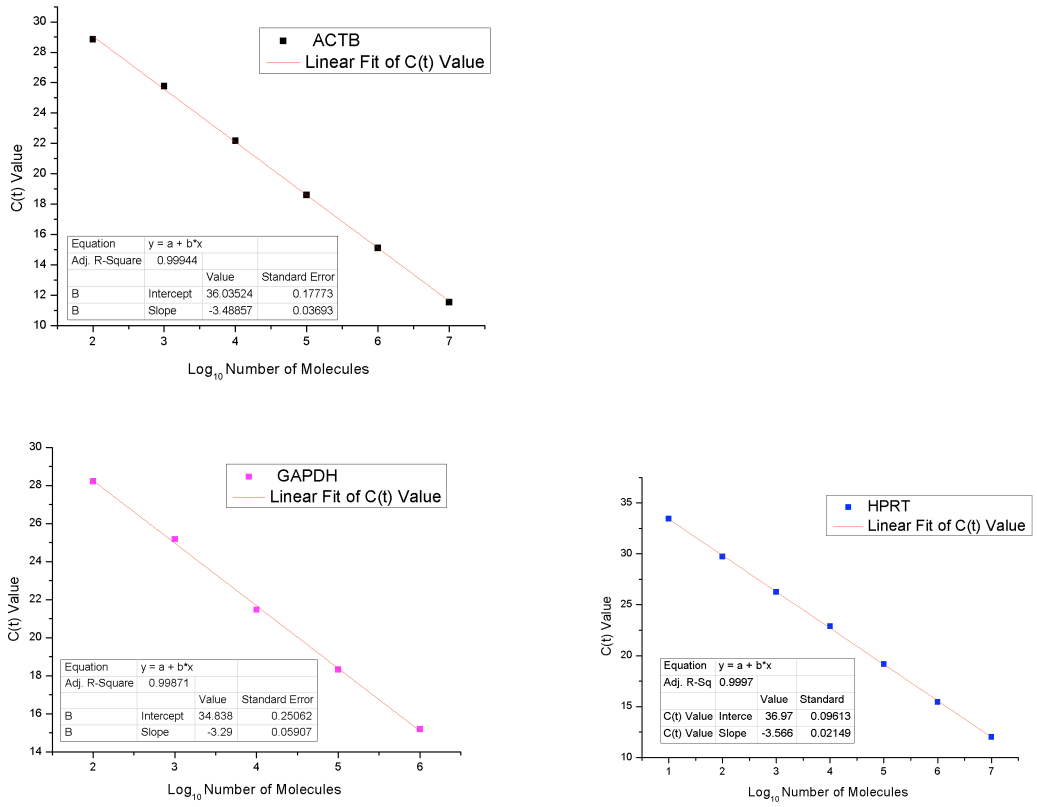

Figure 4.5 PCR standard curves for ACTB, GAPDH and HPRT using synthetic DNA templates

4.4 Effect of AC field in probing efficiency

4.4.1 Compare Hela cell probing results with/without applying AC field

RT-PCR results of mRNA probing from single Hela cells under the applied AC field of 1.5 V_{RMS}, 10 MHz are shown in Figure 4.6, using standard curves, the Ct values were converted into the number of target molecules in this plot. Multiple transcripts, including ACTB and GAPDH with high abundance, as well as HPRT with low copy

numbers are targeted from one probing result. The average extracted copy number of ACTB from a single HeLa cell was 1360, and was 703 and 68 for GAPDH an HPRT, respectively. The control experiments where no AC field was applied during probing showed a much smaller reading. Typically below 100 molecules were detected even for more abundant gene ACTB and GAPDH. For most of the cases, there was no PCR amplification for this set of samples, meaning that the collected molecules were below our PCR detection limit, which was below 100 molecules for ACTB and GAPDH, and ten molecules for HPRT. These results demonstrated the significant concentrating effect with the application of AC filed during probing and the necessity for field application in extracting target molecules from living cell using coaxial probes.

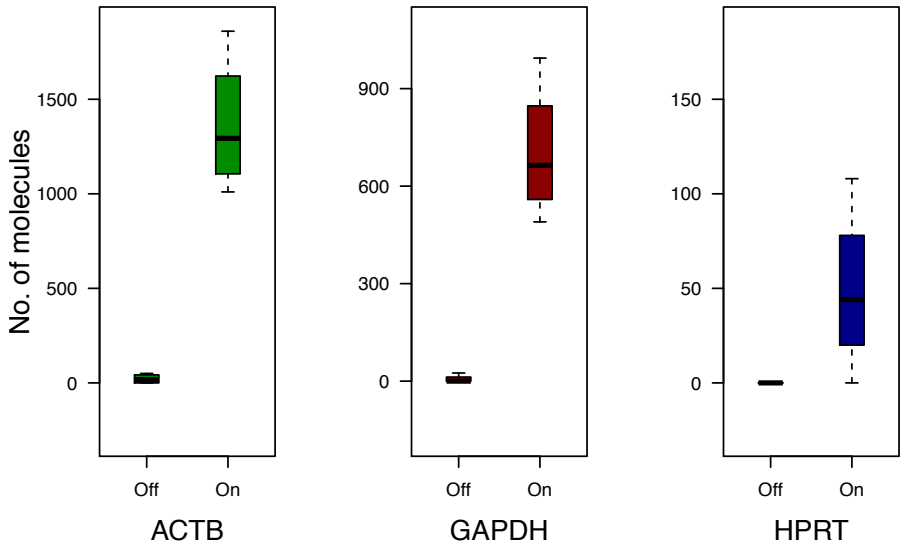

Figure 4.6 Compare probing efficiency with and without applying AC field

4.4.2 Effect of field frequency on probing results

Similar to the in vitro fluorescence experiments with dye-labeled DNA, the in vivo cell probing experiments were performed with applying AC field of different frequencies from 10KHz to 30MHz. Figure 4.7 shows the number of target ACTB mRNA collected using the coaxial probe device with the application of AC field at different frequencies. From in vitro fluorescence experiments with dye-labeled DNA molecules, it was known that the DEP collection worked within a small frequency range with collection-peak around 10~15MHz. Here in vivo cell probing results indicated similar frequency selectivity where probing efficiency was much higher at 10MHz compared with other frequencies. We thus chose 10MHz as applied AC field frequency for all in vivo probing experiments.

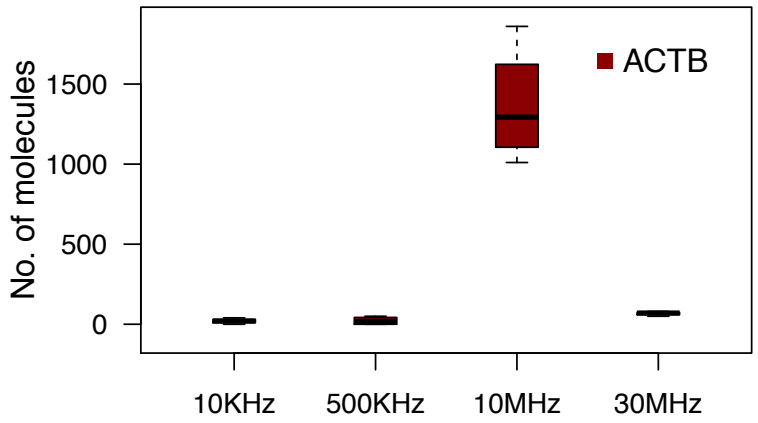

Figure 4.7 Target ACTB mRNA molecules collected with applying AC field at different frequencies

The Ct values of 10 single cell probing results were plotted as the gene-expression heatmap in Figure 4.8 for illustration. The results indicated that the expressions of ACTB and GAPDH were higher than HPRT as expected. The cell-to-cell variations were also shown by different expression levels between each cell. For each target gene, 10% of the total cDNA product was transferred into the qPCR reaction volume. With this current RT-qPCR set up, the expression levels of 10 different genes could be analyzed during specific gene primer set for each single cell probing. However, more genes can be analyzed by increasing the efficiency of the qPCR assay, so that less amount of cDNA product could be used for PCR. Also, sequence-specific fluorescent probes can replace SYBR-Green as the reporting dye; therefore different genes can be quantified at the same time with multiplexing capacities.

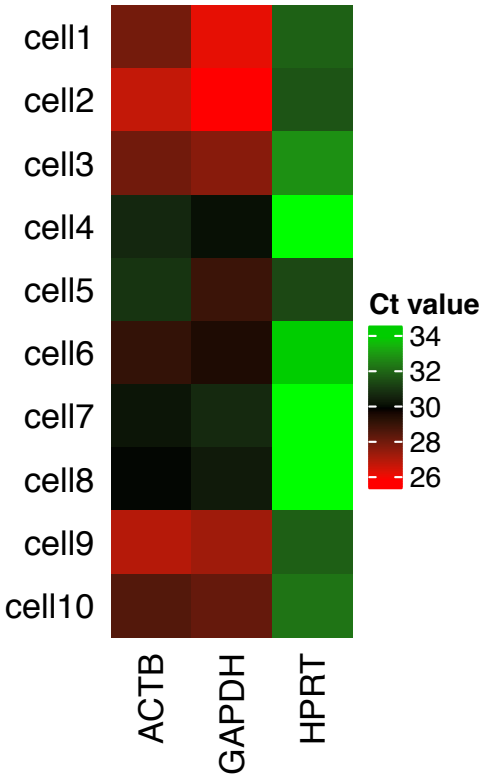

Figure 4.8 Gene expression heatmap based on the RT-PCR results of extracted mRNAs from single cells

4.5 Selectively pick up the whole cell from gel matrix for single cell analysis

4.5.1 The effect of the application of high AC voltage and procedure for whole single cell gene expression analysis

It was found that when the applied voltage on the coaxial probe was greater than 1.9V_{RMS}, the generated DEP force was high enough to pull cell membrane and resulting in a slightly contrast changing in the optical images of the probing cell, as

shown in Figure 4.9. The edge of target cell became darker under the optical microscope when applying high AC voltage, and went back to original contrast when the AC voltage was turned off. Moreover, at this probing voltage, the whole cell could be picked up using coaxial probes as dielectrophoresis tweezers by keeping the high AC voltage on when retracting probe from the gel substrate. A process to selectively manipulate single adherent cell and gene expression study for the whole target cell was then developed as shown in Figure 4.10. Once picking up the target cell, the high AC voltage was turned off; the coaxial probe with target cell attached was then immersed in a droplet of 1.5ul of RNase-free water on PDMS substrate with only part of the cantilever in liquid. The probe was then moved out of the droplet. The target cell was still left in the droplet due to the pulling force on target cell from surface tension at air/liquid interface when moving probe out of the fluid. The droplet was then picked up and pipetted into RT-PCR reaction well for downstream gene expression analysis using standard RT-PCR protocols.

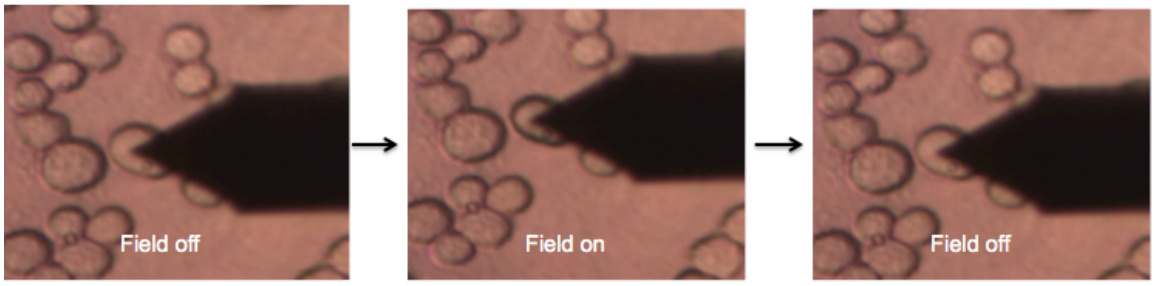

Figure 4.9 Optical image of target cell under probing with and without applying AC voltage of 1.9V_{RMS}

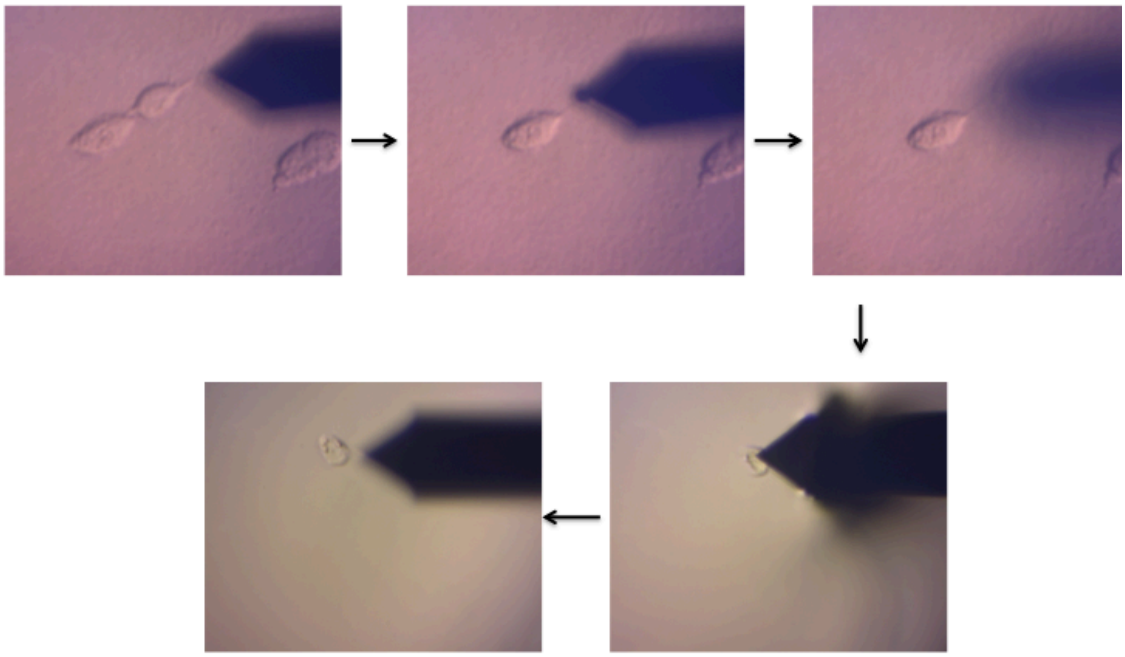

Figure 4.10 Process for selectively picking up single adherent cell on collagen gel and releasing into target droplet for gene expression study

4.5.2 Gene expression analysis with the whole cell probing

Using the as described for the procedure of whole target cells picking up, several single cells were selectively manipulated for RT-PCR analysis. For demonstration, the Ct values of ACTB and GAPDH for ten single whole cells were plotted as gene expression heatmap in Figure 4.11.

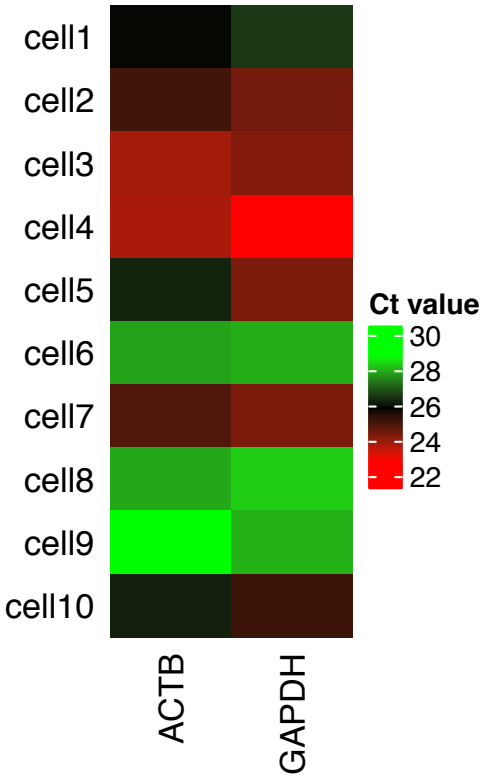

Figure 4.11 Gene expression heatmap based on the RT-PCR results from whole single cells picked up with coaxial probes

4.5.3 Correlations between expression levels of ACTB and GAPDH

Although various housekeeping genes have been used to quantify gene expression in tissue samples, ACTB and GAPDH, are most commonly used to normalize gene expression levels. However, there was evidence that the levels of these two transcriptions could vary in response to experimental manipulation or during different cell stages [83]. There was also evidence suggesting that their uses as internal standards for RT-PCR were inappropriate in some cases [84]. To validate the suitability of these

genes as the reference, as well as validating the probing process with coaxial probes, we compared the Ct values of GAPDH and ACTB in the readings from the whole cell picked up and the readings from mRNA extraction experiments, by determining the degree of correlation between these two gene expressions. The idea behind this approach was that if the gene expressions of these two independently expressed genes tracked each other closely, it would provide enough evidence that they both represented the total amount of RNA in the sample, whereas lack of correlation would indicate that one or both were problematical as reference genes. Also, by comparing correlation coefficient of these two genes between results from extracted mRNA by probing and Ct values from the whole cells, one can evaluate if the results from in vivo cell probing experiments represents relative gene-to-gene relationships in target samples.

Pearson's correlation was introduced as a measure of the strength of a relationship between two variables. The correlation between the Ct value of GAPDH and ACTB were assessed using correlation for readings from the whole cell picked up and mRNA extraction experiments, as shown in Figure 4.12. Ct values of GAPDH were close to those of ACTB for all samples. There was a significant correlation between Ct values of GAPDH and ACTB in the whole cell picked up, with a correlation coefficient of 0.9084264 at p-value= 0.0002751. For readings from mRNA extraction experiments, the correlation between Ct values of GAPDH and ACTB was slightly decreased to 0.8142387 at p-value= 0.0002197, but it still indicated a high correlation between these two genes. This means that the results from in vivo single cell mRNA probing experiments were not random

numbers but actually represented gene-to-gene relationships of target samples.

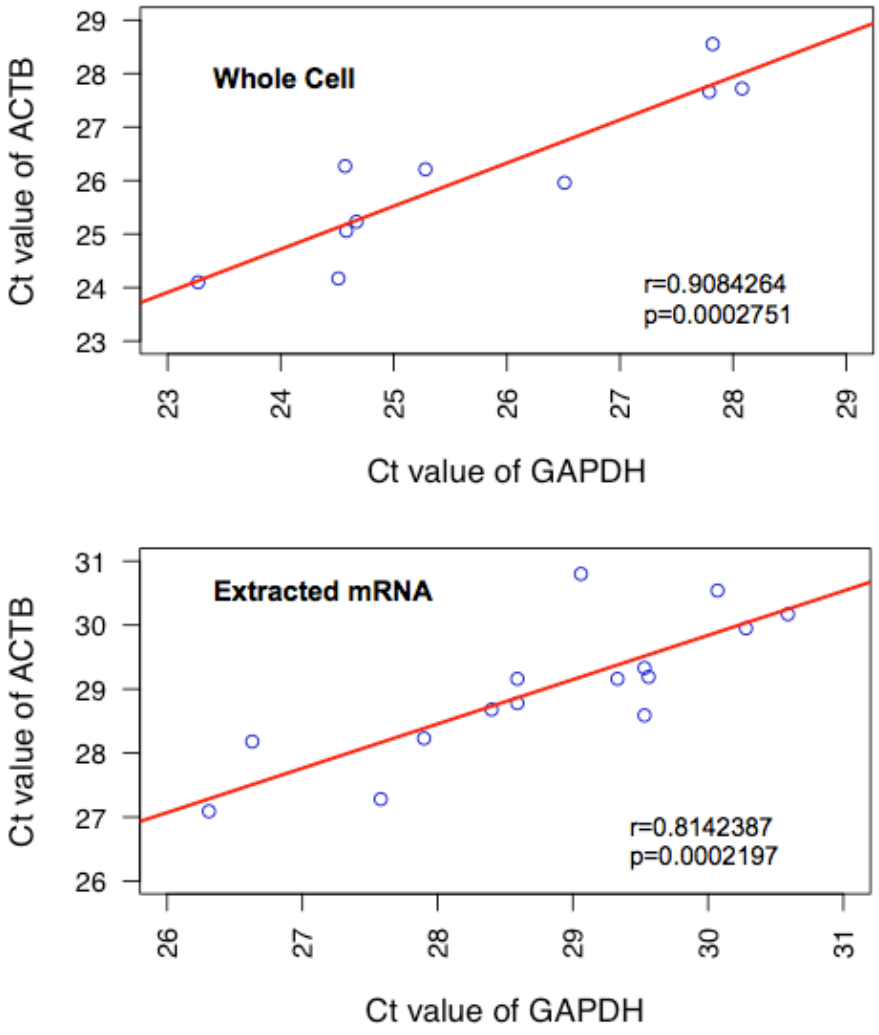

Figure 4.12 The correlation between the Ct value of GAPDH and ACTB using Pearson's correlation for readings from whole single cells as well as readings from extracted mRNA using coaxial probes

4.6 Cell viability analysis after probing

To validate the viability of the mRNA-extracted cells after probing, a live assay was performed with 2 μM Calcein-AM (Sigma-Aldrich) after the probing experiments. Figure 4.13 shows the fluorescence microscopic images of mRNA-extracted cells stained with Calcein-AM. We stained the mRNA-extracted cells with Calcein-AM after 12 hrs of post probing culturing in cell culture dish. The images of single cells showed that live cells could be distinguished clearly by bright green fluorescence. The viability of mRNA-extracted cells probed under the application of lower voltages of 1.5 V_{RMS} was about 50%, lower than the viability of non-probed cells, which was 90% in general. However, the results indicated that the viability of a portion of probed target cells was still preserved, open the possibility for post-probing processes or treatments with the target cells.

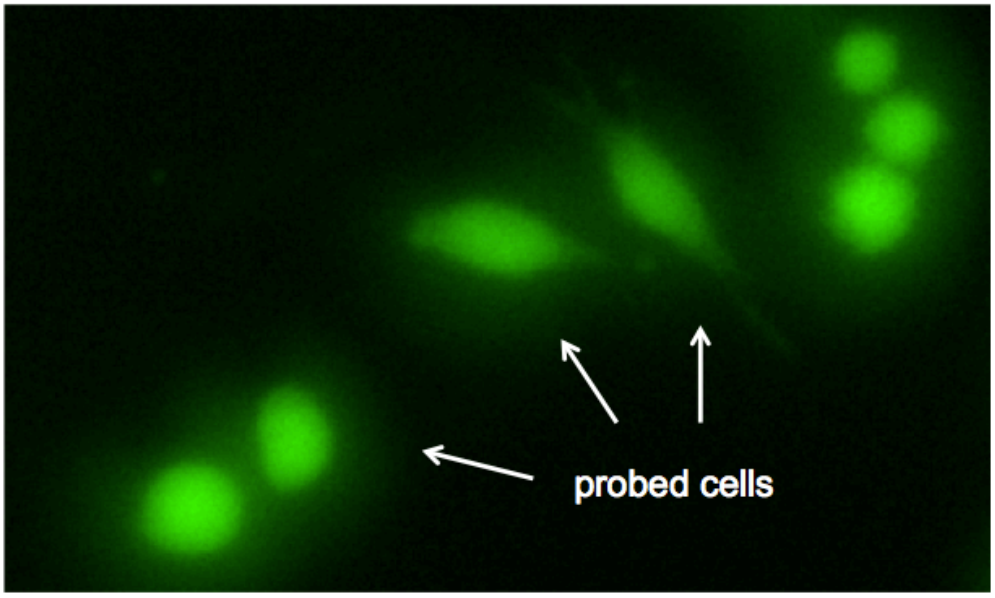

Figure 4.13 Fluorescence microscopic images of mRNA-extracted cells stained with Calcein-AM after culturing for 12 hrs after probing

4.7 Probe reuse by droplet releasing target molecules after probing

A disadvantage of the above-described probing process was that each coaxial nanoprobe was only responsible for one sample reading, which had limitations in perspectives of cost reduction as well as increasing throughput. We thus were working on methods to release target molecules from the probing system, and potentially utilizing well-defined coordinates of target cells and receptacles, integrating the process in a high-throughput manner with added system automation. We had investigated several different approaches for in-situ deposition of mRNA into receptacles from coaxial probes. The initial strategy was to build a heated container stage where one could insert the gold coated coaxial probe tip with

mRNA attached into receptacles such as PCR tubes containing a one-step RT-PCR master mix that could be directly used for PCR assays. The receptacles were heated to 67ºC to release mRNA attached to the probe into the solution. However, we discovered that preheating the mRNA molecules to 67ºC, even for a period of 10 minutes only, resulted in mRNA degradation, and decreased the qPCR efficiency by 100 times.

In a second approach, we examined the feasibility of releasing the mRNA using an external electric field. As mRNA molecules are negatively charged in ideal buffer conditions, the idea was that by applying a DC field between probe electrode surface and receptacles, the target molecules should dissociate from probe surface by electrophoresis. Though initial results based on fluorescence measurements using dye-labeled target molecules were promising, this approach was not successful mainly for two reasons. Frist, the EDTA in standard electrophoresis buffers such TAE or TBE buffers could significantly decrease enzyme activities in downstream RT-PCR reading by forming the complex with magnesium ions in buffers. Second, even if correct buffer recipe had been developed, the electrochemical effect due to applied DC voltage could degrade target mRNA molecules in the releasing process.

Finally, the design for droplet releasing target molecules from coaxial probes after probing was development, by introducing probe surface modifications as well as the vibrations of probe cantilever, as described in the following section.

4.7.1 Droplet releasing concept and setup

The schematic illustration of the droplet releasing process is shown in Figure 4.14. After dielectrophoresis extraction of target molecules using coaxial probes. The probe end was inserted in a droplet of RT (reverse transcription) reagent on top of PDMS substrate. A piezoelectric actuator was added underneath the coaxial probe on the probe holder as shown in Figure 4.16. The actuator drove the probe cantilever vibrated at its resonant frequency around 300KHz for 30s while keeping the probe end inside the droplet. The vibration of cantilever helped target molecules dissociating into RT reagent droplet. As a common strategy to decrease nonspecific binding on the bio-device surface, the probe surface was modified with 2-[Methoxy(polyethyleneoxy)propyl] trimethoxysilane (PEG-Silane) to minimize binding force between target molecules and electrode surface, thus facilitate the releasing process as well. The probe was then retracted from target droplet and immersed in the washing droplet containing RNase-free water, again with driving cantilever vibration on for 30s at the resonant frequency. Another optional washing step with ethanol could be done in the same manner in between these two droplets. The washed probe was then used for subsequent probing. The target droplet was picked up and pipetting into RT-PCR wells for downstream analysis. Optical images of probing and droplet releasing processes are shown in Figure 4.15. In this manner, no probe changing and realignment was needed, and each probe was capable for multiple probing. Utilizing well-defined coordinates of target cells and droplet arrays, the probing process was semi-automated with LabVIEW interface for

higher probing throughput.

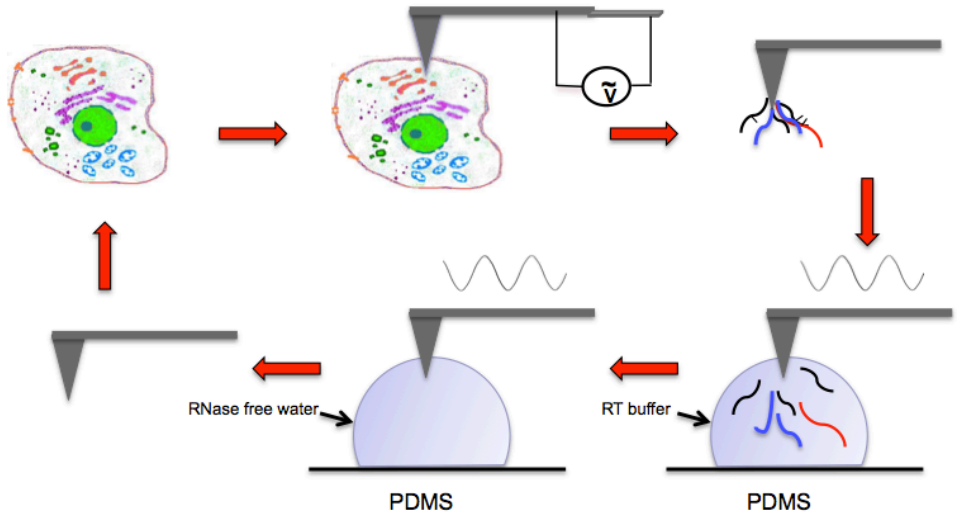

Figure 4.14 Illustration of the droplet releasing process for probe reuse

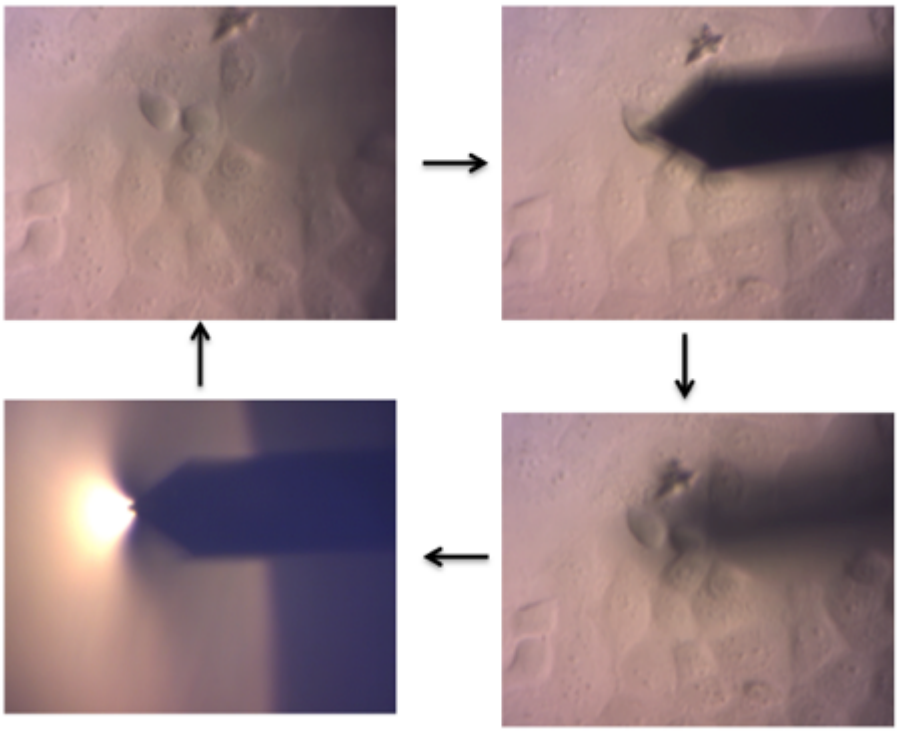

Figure 4.15 Optical images of probing and droplet releasing processes

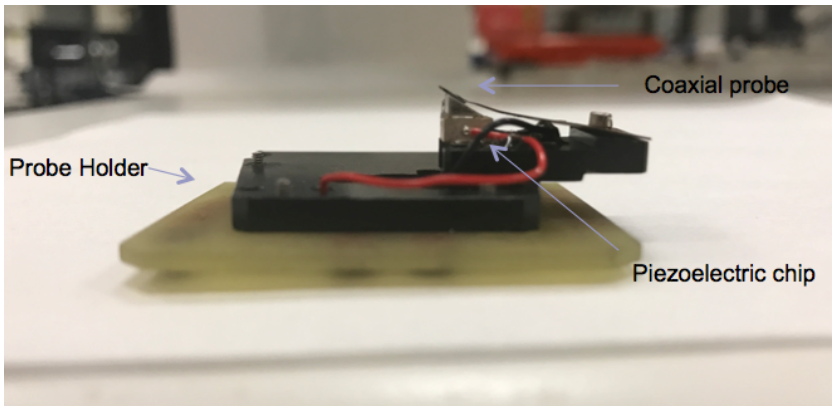

Figure 4.16 Probe holder with the piezoelectric chip attached.

4.7.2 Droplet releasing results and process reliability characterization

To test the releasing efficiency of the above process, the used coaxial probes, after releasing target molecules into RT reagent droplet, was then dropped into PCR tubes to

quantify the number of molecules left on the probe with PCR readings. In this way, for each probing, the numbers of molecules in the releasing droplet and that left on the probe were compared side by side. Such comparison for ACTB is shown in Figure 4.17 as an example. It can be seen that for ACTB, although there were still small portions of molecules left on the coaxial probes, with numbers typically below 100 molecules, the majority of molecules were released into target droplets for tested samples. On average there was about three cycles difference in Ct values between the released droplet and those on probe after releasing. At least 80% of extracted mRNA molecules were released in the RT buffer droplets, and could be analyzed further through RT-PCR.

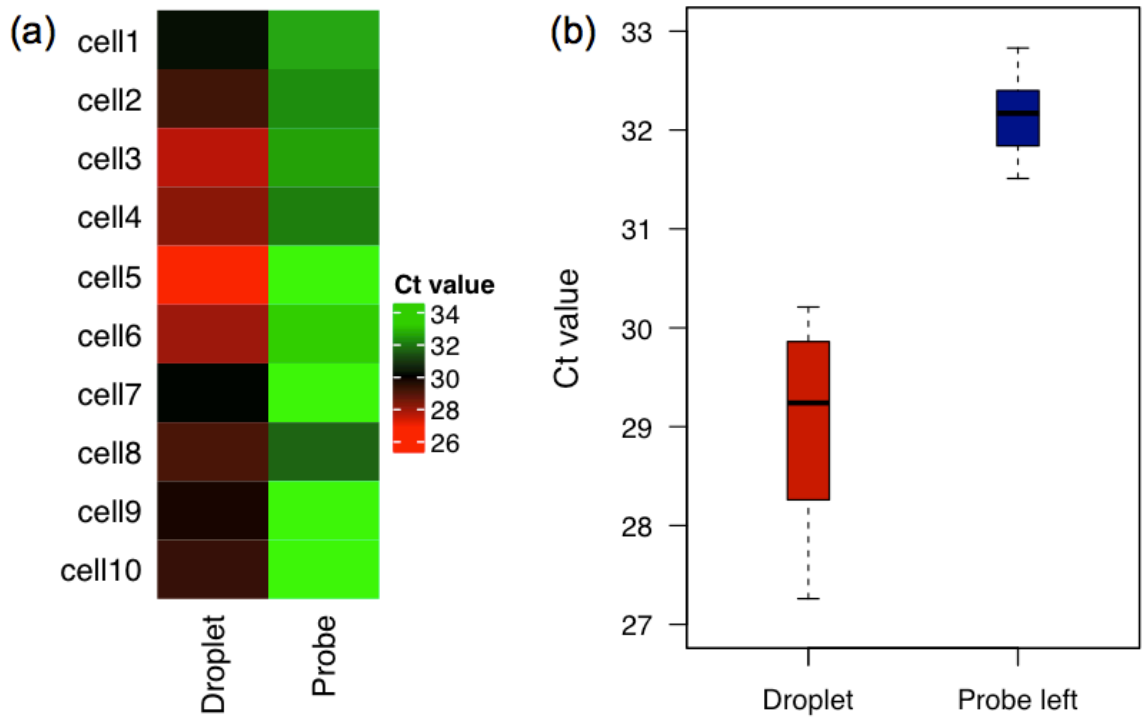

Figure 4.17 (a) ACTB Ct value heatmap comparing target molecules in releasing droplet and those left on probe surface for each probing. (b) Compare ACTB Ct values between target molecules in releasing droplet and those left on probe surface for each probing

4.7.3 Washing efficiency and cross contamination test

To address the effectiveness of droplet washing after targets releasing as well as the degree of cross contaminations between droplet readings, another set of experiments were done as following. After extracting mRNA molecules from a target cell, the releasing process was done in two release droplets of RT reagent in series, wherein between the two releasing droplets, the probe was washed in the washing droplet as described in the previous section. The probe was then ready to be used for probing a second cell, and releasing steps were conducted again in two RT droplets with washing steps in between. These releasing droplets were then pipetted into PCR wells for RT-PCR reading and heatmap of ACTB Ct values for this two types of releasing droplets were plotted in Figure 4.18 for each probing. It can be seen that while the first releasing droplets had readings from released ACTB mRNA, there were absolutely no molecules above PCR detection limit present in the second releasing droplet. This means that the washing steps successfully removed the target mRNA molecules that left on the coaxial probe surface after first releasing. There was absolutely no cross-talking between droplet readings. Each reading in the droplet one series was from the target cell probed before releasing.

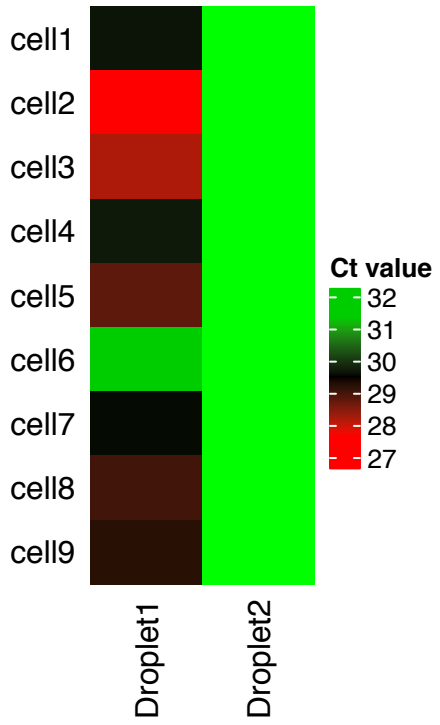

Figure 4.18 Heatmap of ACTB Ct values from two types of RT releasing droplets where washing steps were added in between each releasing. The probes only inserted and extracted mRNA molecules in target cells before first releasing in Droplet1. There was no probing event before releasing in Droplet2. Results with no PCR amplification were plotted in light green

4.7.4 The correlations between gene expression levels of target cells and Ct readings in releasing droplets

Although in the previous section we have compared correlations of ACTB and GAPDH Ct values for extracted mRNA using the coaxial probe and the whole cell mRNAs, and readings from the probing process indeed reported gene-to-gene relationships of target samples. This is not a direct evidence demonstrating that the readings from each probing accurately represents gene expression levels in the tested cell. Thus another set of experiments was performed as following. After probing the target cell as well as the

droplet releasing and washing processes, the probe was moved back to the sampled target cell, and the whole sampled cell was picked up from gel by increasing applied field and analyzed with RT-PCR as described in the previous sections. In this way, the probing results of a target cell in RT releasing droplet was compared, side by side, with the readings from the contents left in the target cell after probing, for both ACTB and GAPDH.

Pearson's correlation was again introduced to measure the correlations of the Ct values between the releasing droplet and the whole cell left after probing, as shown in Figure 4.19. There was a significant correlation between Ct values of ACTB between releasing droplets and the sampled whole cell, with a correlation coefficient of 0.809868 at p-value= 0.0001433. For readings from Ct values of GAPDH, the correlation coefficient was 0.8373504 at p-value=0.001299. On average there was 3.2 cycles difference for ACTB Ct values between releasing droplet from extracted mRNA and sampled the whole cell. The difference was 3.1 cycles for GAPDH Ct values. This corresponded a ratio of about 10 to 1 between contents of a target cell and extracted mRNA with the coaxial probe, if assuming reading in releasing droplet and sampled the whole cell shared the same RT-PCR efficiency and target material loss. The high correlations between releasing droplet readings and that of target cells indicated that the final probing results obtained from releasing droplets were capable to truly reflect gene expression levels of the target cells.

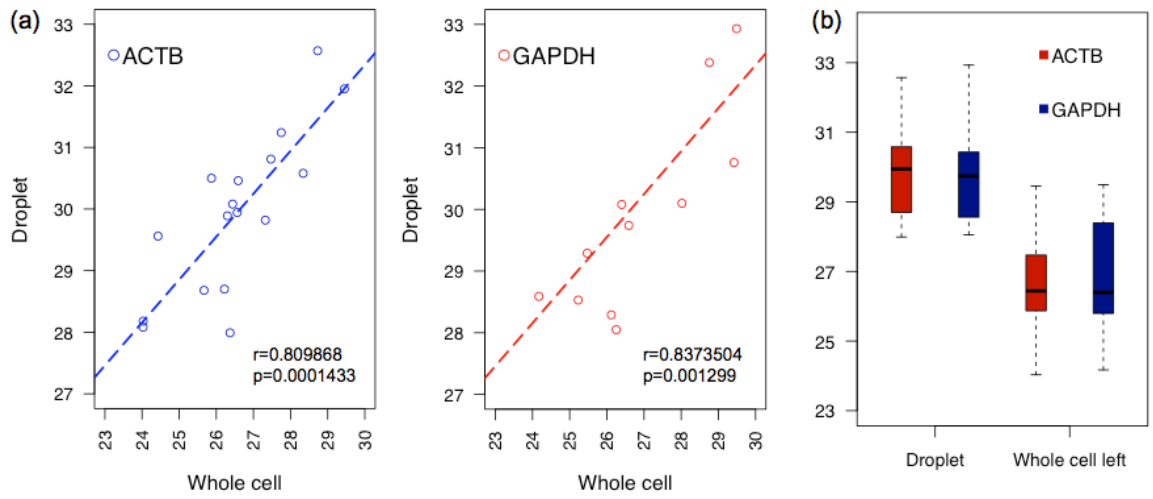

Figure 4.19 (a) the correlations of ACTB and GAPDH Ct values between each releasing droplet and sampled the whole cell after each probing. (b) compare Ct values of ACTB and GAPDH bet between each releasing droplet and sampled the whole cell

4.8 Explore the possibility of multiple probing for a target cell

With the above quality control tests for the probing and target releasing processes, we further explored the possibility of multiple probing for a target single cell. For this set of experiment, the target cells were sampled twice, and the extracted mRNA molecules were releasing in two RT buffer droplets with washing steps in between. The time interval between the two probing was around five minutes for each target cell. The initial results of extracted ACTB values for two-time probing from the same cell were plotted in Figure 4.20.

The results demonstrated the capability to target and sample mRNA molecules for two times within a single living cell. This opened the possibility of dynamic tracking gene expressions on single cell level by bringing time parameter in gene expression studies, while with PCR level of sensitivity. By providing reliable and exceptional sensitivity to

identify differences between individual cells in a seemingly homogeneous population, the system creates possibilities for assaying the genomic analysis in living cells and tracking them in response to external stimuli such as drugs or cell signaling molecule, as well as retrieval of target cells after analysis.

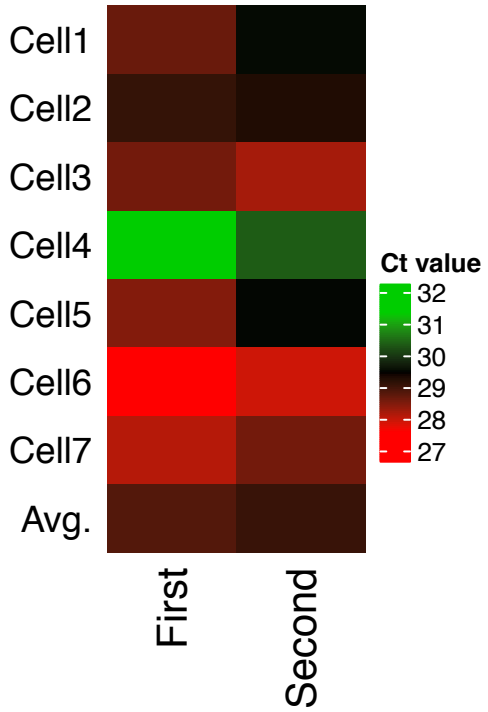

Figure 4.20 Heatmap of ACTB Ct values extracted from two-time probing of the same cell

4.9 Summary

In this chapter, we described a unique instrument for cell biology – single cell analyzer that coupled nanoscale dielectrophoretic probe technology with RT-PCR technique for in situ single cell gene expression analysis. The developed bench-top instrument utilized modified AFM coaxial probes for the extraction of intracellular molecules from cell samples. The adherent cell samples were cultured on collagen gel for select-and-probe analysis. The AFM coaxial probe served as nanotweezer, and wherein the application of an alternating potential between the inner and outer electrodes of the coaxial probe creates a dielectrophoretic force for attracting target molecules toward the tip-end. The technology directly targets and non-destructively samples mRNA expression levels down to less than 100 molecules within a single living cell without the need for purification and averaging typically of conventional technologies. The ability to quantify mRNA transcripts as a function of space and time is a capability that was not available to the biologists today. We believe that this technology has the potential to transform cell biology in a profound way – by tracking quantitative studies and spurring many areas of investigation in biology. These include understanding the heterogeneity of transcriptional responses and its implications for cell function and disease, differential mRNA transport, and localization in neurons, as well as epigenetic regulation, stem cell development and tumor biology.

CHAPTER 5 INTEGRATED MICROFLUIDIC-AFM PLATFORM FOR SINGLE-CELL ANALYSIS

5.1 Introduction and concept description

A variety of microfluidic platforms have been developed to analyze single cells from genotype to phenotype, however, most of the established methods, e.g., single-cell sequencing [85], RNA sequencing [86], single-cell RT-qPCR [87] and droplet PCR [88] require cell lysing and complicated purification procedures to isolate genetic materials from single target cells. As these methods require destroying the cells, they are not suitable for either comparing the gene expression of single cells before and after external stimulation, or releasing stimulated cell for further analysis.

In this chapter, an integrated microfluidic/nanoprobe platform for tracking expression levels of target molecules in single live cell within a population of cells is presented, in which cells are trapped in an ultra-thin polydimethylsiloxane (PDMS) membrane-sealed chips and produces single-cell arrays for probing. It utilized the coaxial probe device to penetrate through the membrane and extract mRNAs from target cells. This trap and probe technique provides no needs of complex cell selectively release process for downstream analysis, renders a perfect approach for single CTCs study with no WBCs background contamination. HeLa cell trapping and probing

experiments demonstrated cell viability after gene expression analysis, which is the first to facilitate the direct, in situ collection of transcriptional profiles from single cells of interest from a sealed microfluidic device with minimal impact to cell viability.

5.2 Platform design

The schematic illustration of the platform is shown in Figure 5.1a. It consisted of a membrane-sealed microfluidic chip for high throughput single-cell trapping and the modified AFM nanoprobing system for the extraction of intracellular mRNA molecules from an individual living cell. The design of the microfluidic single-cell array is referred to the design principle reported in [89] which has a 5-row serpentine channel with 20 grooves arrayed along the channel edge of each row (Figure. 5.1b). For each trapping unit, the height of the trap (h_T) is smaller than the height of the delivery channel (H), generating a gap area ($h_G = H - h_T$). Therefore, there is a perpendicular stream flowing through the gap, crossing each row of the delivery channel and pushing cells into traps. At the turning zone of each row, there are dummy traps, which do not catch cells but help generate perpendicular flow for cell focusing. Cells are delivered to the traps sequentially by the horizontal delivery flow, and pushed into the traps by the perpendicular pushing flow. As the trap size is similar to the cell size, once occupied by a cell, it physically excludes the next cell and reduces the possibility of trapping multiple cells.

The single-cell array was sealed with an ultra-thin PDMS membrane, which allows coaxial probes, as external instruments, to penetrate through and access or analyze a particular single cell. After cells had got trapped in the membrane-sealed single-cell array, the chip was placed onto an upright microscope, and the modified AFM probe was controlled by the micro-motor to move to the target cell and extract the cells mRNA. The principle of single-cell mRNA probing is explained in Figure 5.1c. After penetrating the ultra-thin sealing membrane and reach inside cell with coaxial nanoprobes, application of an AC electric field between the inner (silicon core) and outer metal electrodes of the probe created a large electric field gradient, resulting in a dielectrophoretic force strong enough to attract mRNAs to the probe-end. The probe then retracted from trapping chips and drop into tubes with RT-PCR reagent for quantitative gene expression analysis. During this step, the fished out molecules dissociated from probe surface and got amplified in PCR process.

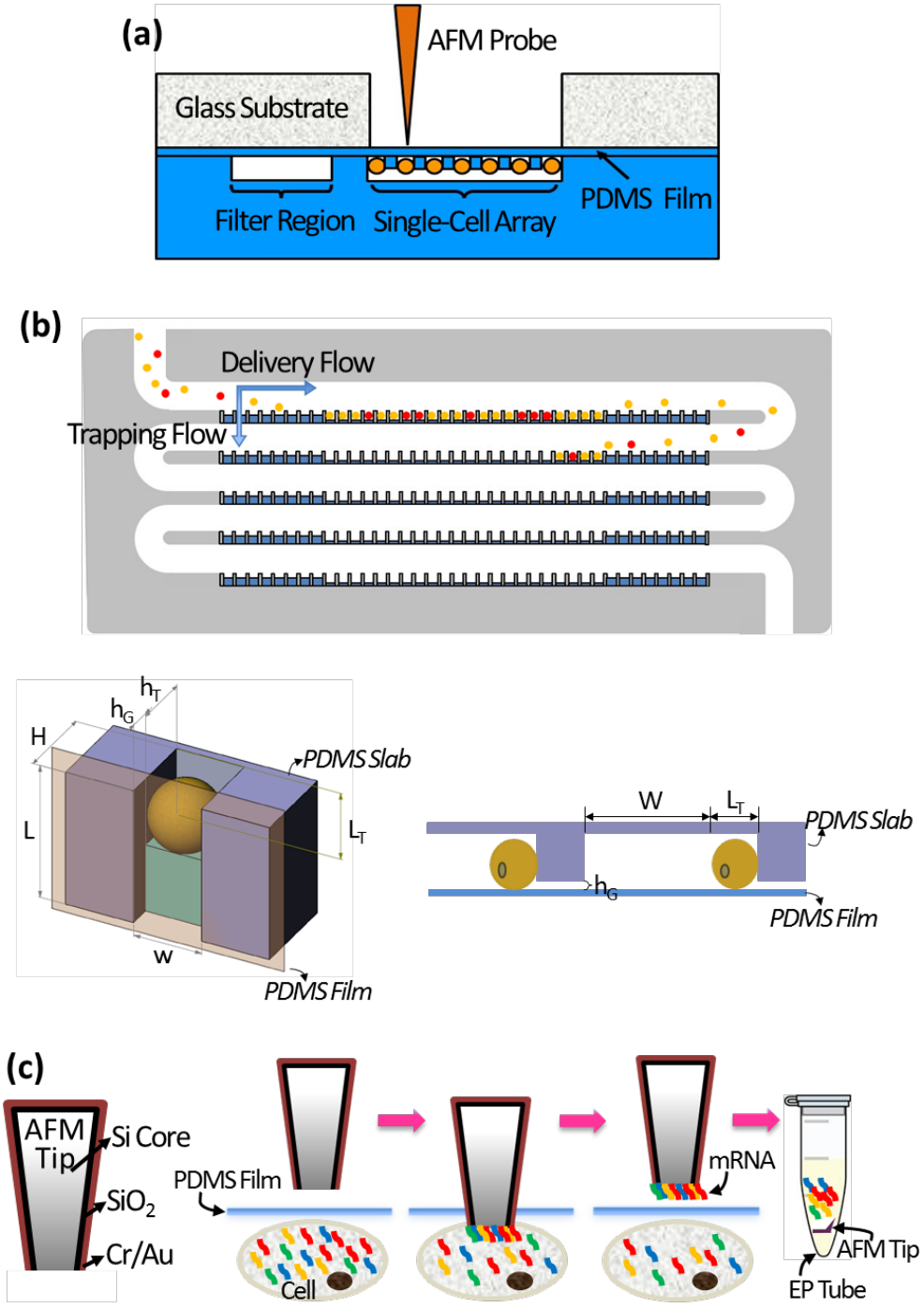

Figure 5.1 Schematic representation of (a) the proposed microfluidic platform and (b) the design of the microfluidic single-cell trapping array. (c) The process of single-cell mRNA extraction by a modified AFM probe. mRNAs responding to the AC field of 1.5 V and 10 MHz between Si core and Cr/Au nanolayer are attracted to the probe-end,

picked out from the target cell, and quantified by RT-PCR to analyze the single-cell expression level of target genes

5.3 Assembly of the microfluidic chip

The device assembly procedure is illustrated in Figure 5.2a. Bond-detach lithography[90] was used to seal the PDMS microfluidic device with an ultra-thin PDMS membrane. The ultra-thin PDMS layer was fabricated by spin coating and heat curing of PDMS pre-polymer mixture's hexane diluent on a Teflon® coated silicon wafer. Teflon® coating efficiently reduced the adhesion of PDMS to silicon wafer to facilitate an easy peeling off of the sealed device; while diluting PDMS pre-polymer mixture in hexane reduced its viscosity, so that a much thinner membrane could be produced at similar spin coating parameters [91]. Figure 5.2b summarizes the resulting membrane thickness according to the ratio of hexane to PDMS pre-polymer at the spin coating condition of 5000 rpm for five mins. The final thickness of the PDMS membrane used in the platform was chosen to be 1µm (measured by Dektak 3 Profilometer), which was fabricated by spin coating PDMS and hexane mixture at a mass ratio of 1 to 2. Optical images of the ultra-thin PDMS membrane, the fabrication procedure, and a finished device are shown in Figure 5.2c.

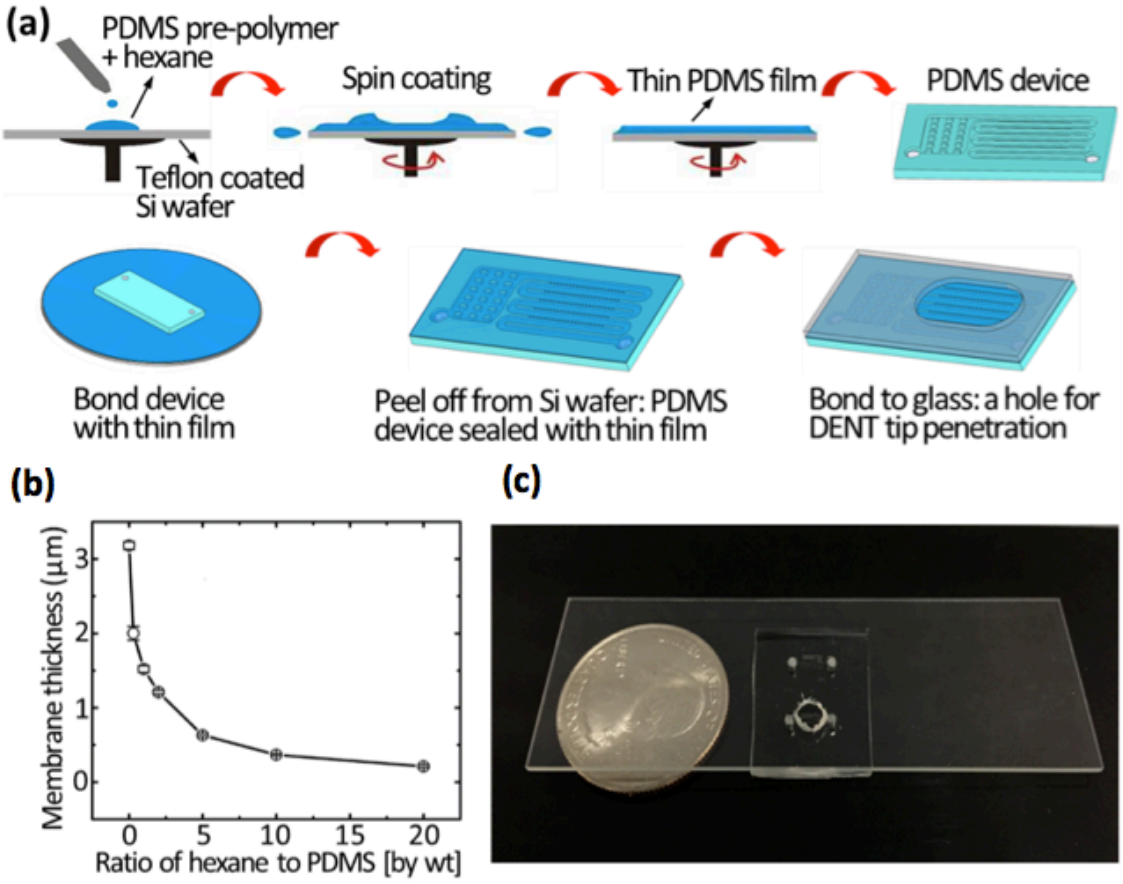

Figure 5.2 (a) Fabrication process for the ultra-thin PDMS membrane-sealed single-cell array. (b) The thickness of the PDMS membrane according to the different ratios of PDMS pre-polymer to hexane at the spin coating conditions of 5000 rpm for 5 min. (c) Optical image of the assembled device

5.4 Microfluidic chips design results of single-cell trapping

For initial proof of concept demonstration, we started with trapping HeLa cells to investigate device trapping efficiency as well as the feasibility of gene profile analysis for trapped target cells. The trapping efficiency of the membrane-sealed microfluidic single-cell array was tested using HeLa cells with a diameter of around 15 µm, which have cell size in a similar range as CTCs. Different channel design parameters were tested

experimentally, and the trapping result with the optimized parameter is shown in Figure 5.3. Up to 98% single-cell occupying efficiency was achieved, with an average single-cell occupying efficiency of 94%±4%. For the optimized design, the trap width (W_T) was set to be 15 μm (similar to the target cell diameter), the delivery channel height (H) was 18 μm, the gap height (h_G) was 4 μm, and the delivery channel width (Wd) was 60 μm (four times of the target cell diameter). At a HeLa cell concentration of 1×106/mL, and a flow rate of 2 μL/min, 100 HeLa cells were sequentially and deterministically within 20s.

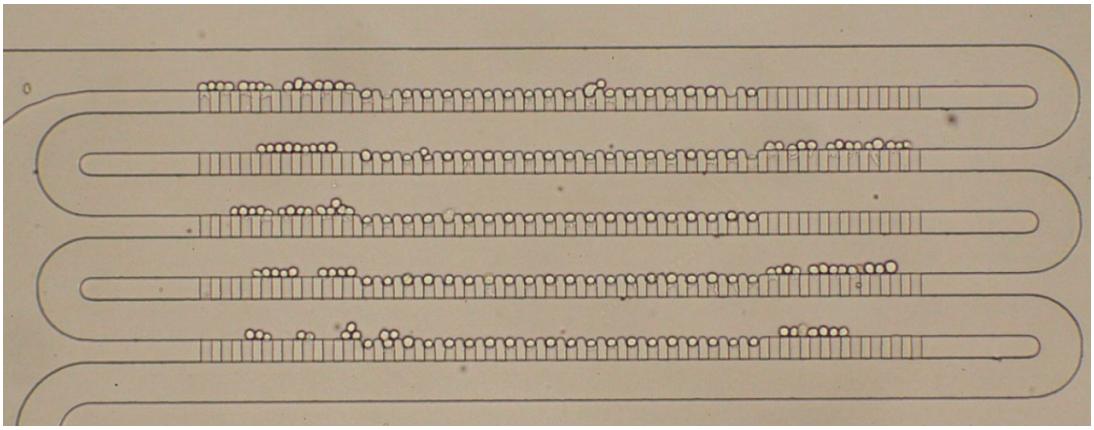

Figure 5.3 Bright-field image of trapping of 100 single HeLa cells within the ultra-thin PDMS membrane-sealed single-cell array

5.5 Probing of Dye-labeled cell trapped inside microfluidic channels

The bright field images recording the procedure of single-cell mRNA probing is shown in Figure 5.4. Upon placing the microfluidic device under an upright microscope and on top a motorized probe-holding stage, the modified coaxial probe was moved by the micro-motor to a selected cell of interest, followed by penetrating through the membrane and entering into a specific cell. The contact detection between the probe

and the PDMS membrane could be easily observed by the membrane deformation under a microscope. Once contact was established, short voltage pulses were applied to the probe control motor to move the probe down in pulse steps, so that the probe was able to penetrate through the membrane and insert into cytoplasm with controllable penetration depth. The penetration move stopped when probe punched trough the ultra-thing sealing membrane, indicated by an apparent relaxation from cantilever bending.

Once the probe-end completely penetrated the cell membrane, the AC field between inner and outer electrodes was turned on, and mRNAs were attracted toward the tip-end by DEP force. After 75 s, the probe was retracted from the cell, the AC field was turned off, and the extracted mRNA molecules were released for RT-qPCR to obtain the cell's gene expression fingerprint. To verify that the tip was inserted into the cytoplasm, it was controlled to penetrate into a Calcein AM-stained Hela cell, and fluorescence molecules of Calcein AM were successfully detected at the tip-end under an upright fluorescence microscope (Figure 5.5), indicating the probe was able to penetrate through the membrane and insert into the cytoplasm.

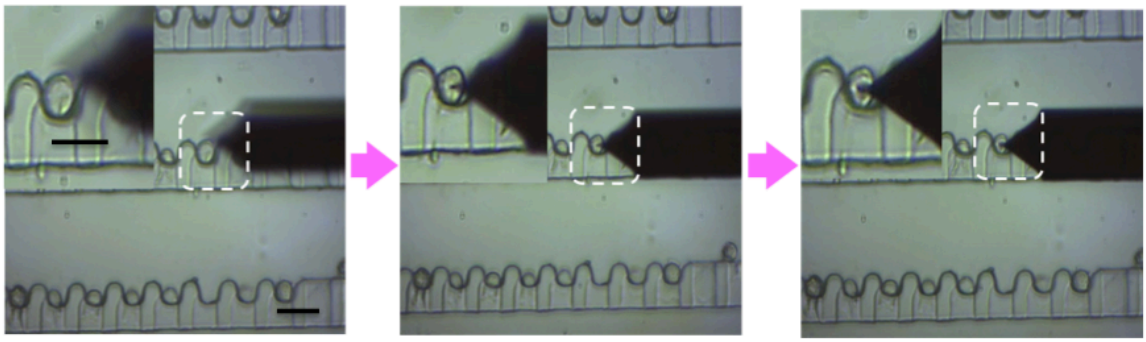

Figure 5.4 Bright-field microscopic images representing the single-cell probing process. White dashed box indicates the cell of interest. The probe was moved downward toward a target cell, penetrated through the PDMS membrane and inserted into the target cell to extract mRNAs by DEP force. Scale bar 30 μm

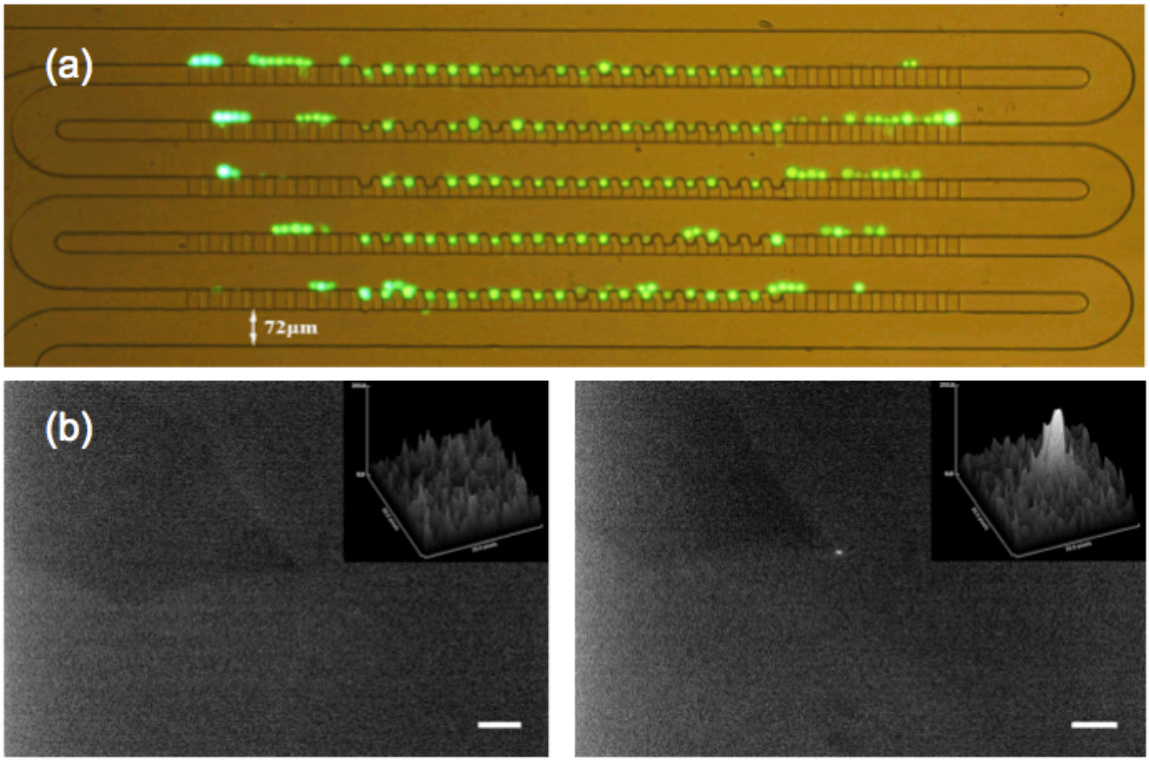

Figure 5.5 (a) Combined bright-field and fluorescence image of Calcein AM-stained HeLa cell within the ultra-thin PDMS membrane-sealed single-cell array. (b) Fluorescent images of the coaxial probe end before (left) and after (right) penetration into a Calcein AM-stained HeLa

5.6 Experiment results of field strength effect for in vivo probing inside microfluidic channels

For in vivo probing experiments, 100 HeLa cells were trapped in the single-cell array, and the single-cell expression level of 3 housekeeping genes, ACTB, GAPDH, and HPRT were analyzed based on RT-qPCR results of extracted mRNAs by the probing of trapped single HeLa cells. For each different gene, 10% of the total cDNA product was put into the qPCR reaction volume as suggested by manufacturer protocol. It was found that the amount of mRNA molecules picked up, as from reading in qPCR results, were controlled by the amount of voltage across the inner and outer electrodes of coaxial nanoprobes. As the applied voltage increased, the extracted number of mRNAs increased dramatically. This indicated stronger DEP effect and higher fishing out efficiency associating with elevated voltage application. At the AC condition of 1.1 VRMS at 10 MHz, small numbers of ACTB (mean CT = 31.4, SD = 1.1) and GAPDH (mean CT = 32.3, SD = 0.7) mRNAs were extracted and there was no HPRT reading. At the applied voltage of 1.5 and 1.9 V, all three types of mRNAs were successfully detected, but more ACTB and GAPDH mRNA molecules were detected than HPRT because of their inherent expression level differences, considering ACTB and GAPDH are abundant genes while HPRT has low expression. The absolute number of molecules extracted of different genes at different voltage was calculated based on the above RT-PCR CT values and standard curves, as is shown in Figure 5.6. The number of ACTB mRNA was around

350±170 at 1.1V, 3730±960 at 1.5V, and 7590±1260 at 1.9V; the number of medium abundant gene GAPDH mRNA was 100±30 at 1.1V, 740±390 at 1.5V, and 2940±870 at 1.9 V. As for the low-expression housekeeping gene HPRT, there was no reading at 1.1V, 40±10 molecules were extracted at 1.5V, and 90±40 molecules were extracted out at 1.9V. These results showed that our platform has tunable target signal intensity with respect to applied voltage. The ability to probe and detect low copy number HPRT mRNAs is critical as it may benefit CTCs analysis when target molecules are rare or at the low expression level. Controls for reading from probing microfluidic channel only but not going inside cell showed a negative reading with no amplification.

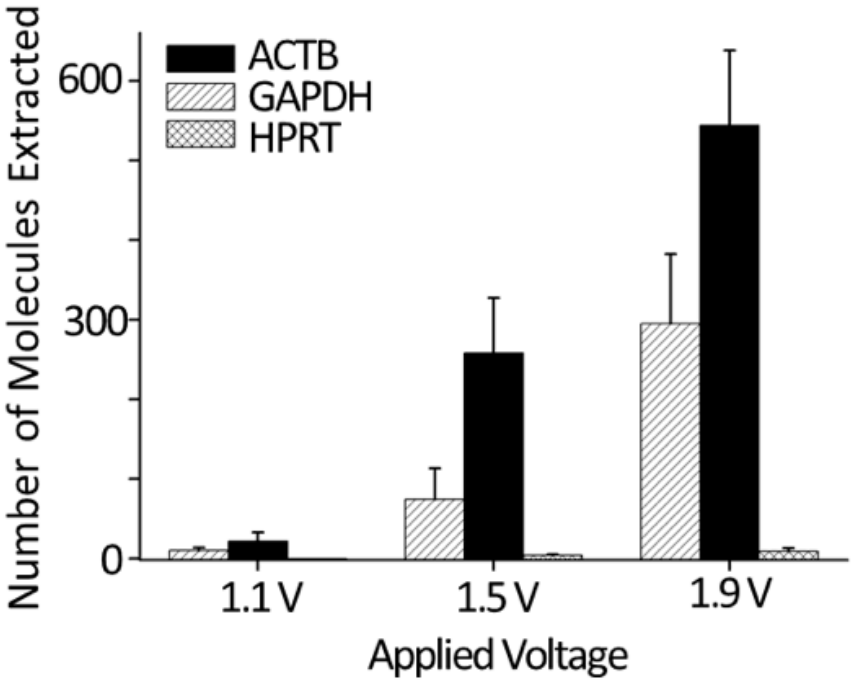

Figure 5.6 The calculated absolute numbers of extracted mRNAs under an applied voltage from 1.1 to 1.9 VRMS based on the above Ct values of the RT-PCR experiment and standard curves

5.7 Cell viability analysis at different probing voltage

A cell viability assay was performed to see if the mRNA-extracted cell is alive in the microfluidic channel. Figure 5.7 shows the bright-field and fluorescence microscopic images of Calcein AM-stained cells after probing. The mRNA-extracted cells were stained with Calcein AM after 12 hrs on-chip culture. Bright field and fluorescence microscopic images of single cells showed that live cells were distinguishable clearly by their intact morphology and bright green fluorescence. The viability of mRNA-extracted cells probed under the application of lower voltages such as 1.1 and 1.5 VRMS was ~70%, which was similar to the viability of non-probed cells. However, the mRNA-extracted cells probed under the application of higher voltages like 1.9 V_{RMS} had much weaker green fluorescence signal. This was because a large number of mRNA molecules were extracted by the coaxial probes, damaging the cell metabolism. No cell adherence or proliferation was observed during the culturing of mRNA-extracted cells, and most of the non-probed cells did not adhere to the microchannel bottom or proliferate, either. One possible explanation was that the channel height was ~18 μm, too narrow to supply enough nutrition and space for growing cells. In fact, most microfluidic devices which allow on-chip cell culture have a channel height of above 100 μm [93]. Although probing makes a physical disturbance to the cell membrane, we believe that with an applied voltage of smaller than 1.5 V_{RMS}, cells can maintain the intact cell morphology and viability after mRNA extraction. The fact that the probed samples are preserved with variability after gene expression analysis opens the possibility for further downstream

test, such as in situ drug screen. This may be especially important and beneficial for diagnosis and therapeutic strategy selection, when real time single cell analysis and drug devolvement study is feasible.

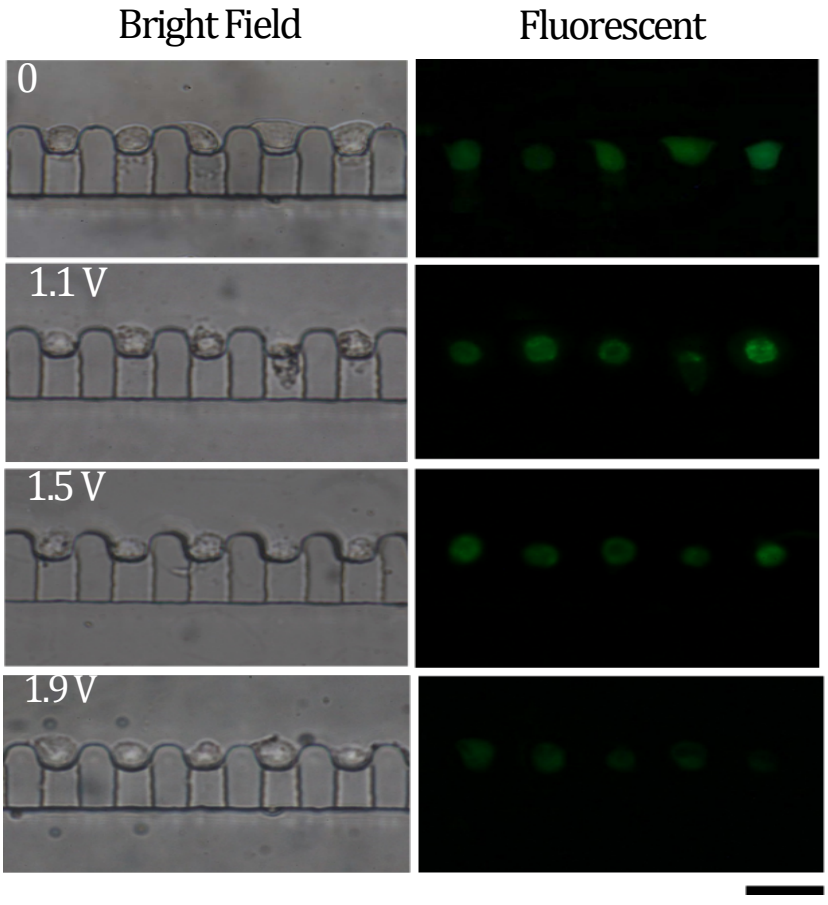

Figure 5.7 Bright-field and fluorescence microscopic images of mRNA-extracted cells stained with Calcein-AM after on-chip culturing for 12 h, respectively. Scale bar: 30 μm

5.8 Perspectives in single-cell diagnostics for circulation tumor cell (CTC)

To demonstrate the perfectives of our platform in CTC analysis where target CTCs is often in a mix with background WBCs after microfluidic enrichment. The integrated platform was then applied to cell type identification as well as single cell analysis in an artificial cell mixture. For this set of experiments, SK-BR-3 and U937 cells were first introduced into the device at the same concentration of 1×10^6 cells per mL, mimicking a blood sample that underwent primary CTC enrichment (Figure 5.8a). After samples are trapped at particular trapping sites, gene profiles of interested single cell samples were obtained through in situ probing in a select-and-probe manner. SK-BR-3, a human breast cancer cell line, expresses EpCAM (epithelial cellular adhesion molecule) as a CTC marker [93], and over-expresses HER2 (human epidermal growth factor receptor 2) as a breast cancer cell marker [94]. Whereas U937 is a human monocyte cell line, representing the dominant type of WBCs in human blood. It expresses CD45 as a leucocyte marker [95], does not express EpCAM [96], and should have much lower HER2 expression level compared to breast cancer cells [97]. The averaged single-cell mRNA probing results, match with the above marker gene expression status reported in the literature. With the applied AC field of 1.5 V_{RMS}, 10 MHz, mRNAs of EpCAM (Ct = 30.8, SD = 1.3) and HER2 (Ct = 27.1, SD = 1.0) were successfully extracted from SK-BR-3 cells by the coaxial tip without CD45 reading. Whereas for U937 cells, CD45 (Ct = 33.4, SD = 0.5) was extracted, but there was no EpCAM reading and a much lower HER2 reading (Ct = 36.1, SD = 1.3). ACTB from both of the two types of cells was quantified by RT-qPCR as

the positive control. Based on the mRNA expression results plotted in Figure 5.8b and c, although the two types of cells are in a similar size range and could not be differentiated easily from the optical images, the RT-PCR fingerprint of a specific single cell's mRNAs extracted by coaxial probe reveals its specific gene expression levels and cell identity. Figure 5.8d shows the gene expression heatmap [98] representation of 12 single cells. There exist apparent differences in gene expression between SK-BR-3 and U937 cells, and also cellular heterogeneity within the same population. With the ability to plot expression profile of target cancer cells, it might be possible to identify the tissue origin of CTCs by the detection of organ-specific metastatic signatures from the cells, which is helpful to localize small, occult metastatic lesions and to guide further diagnostic and therapeutic strategies.

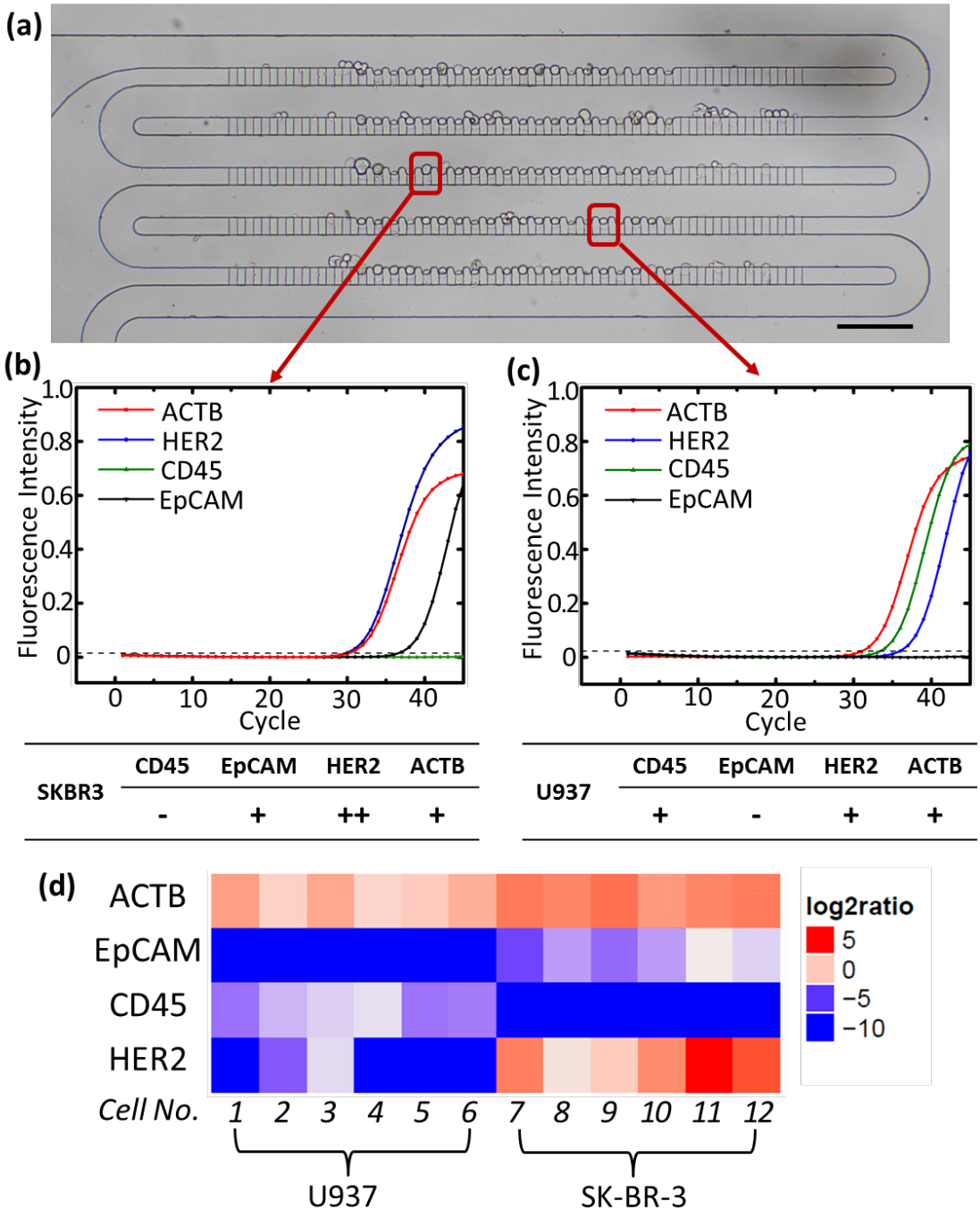

Figure 5.8 Identification of the cancer types for single cells by their marker-genes' expressions using the microfluidic trapping and in situ mRNA probing platform. (a) Bright-field image of trapping single cells of SK-BR-3 and U937 in the microwell array. The RT-qPCR fingerprints of the four target mRNAs (CD45, EpCAM, HER2 and ACTB) extracted by the coaxial probe from a trapped SK-BR-3 cell and a trapped U937 cell

were shown in (b) and (c), respectively. (d) Normalized gene expression heatmap of trapped single cells based on the RT-qPCR results of extracted mRNAs

5.9 Summary

In this chapter, a method was described to extract mRNAs from single living cells in situ, which was a combination of the microfluidic single-cell trapping and the selective intracellular probing using coaxial probe devices. An ultra-thin (~1 μm) PDMS membrane ensured a closed microfluidic environment, thus decreasing the chance that media were accidentally evaporated, and single mammalian cells were isolated individually. 100 single cells were successfully trapped in the size-selective single-cell array within 20 s, with average single-cell occupancy of 94 ± 4%. After the single-cell isolation within the microwell array, the coaxial probe tip was accurately located by the motorized micromanipulator and penetrated through the ultra-thin PDMS membrane to extract mRNA molecules from cell cytoplasm with minimal damage by dielectrophoresis upon the application of AC field. The mRNA probing efficiency, which was related to the amplitude of the applied AC field, was analyzed based on the RT-qPCR results of 3 house-keeping genes, i.e., ACTB, GAPDH, and HPRT, after in situ mRNA extraction, with the post-probing cell viability examined by Calcein AM staining. Also, fingerprinting of the cell-specific marker genes (EpCAM, HER2, and CD45) and differentiation of two different cell lines (SK-BR-3 and U937) were successfully achieved using the proposed platform. The proposed selective, label-free, and non-destructive probing platform

would have a myriad of application areas such as stem cell biology, drug response monitoring, and cancer diagnostics.

CHAPTER 6 CONCLUSION

6.1 Conclusion and future direction

Individual cells within a population are unlikely to behave all in the same way. Current standard techniques are unable to detect within a population of adherent cells and address cell-to-cell differences that can result from genetic variation, biological noise and different characteristics of genes within a population. In this work, we described a unique instrument for cell biology-single cell analyzer that coupled nanoscale dielectrophoretic probe technology with RT-qPCR technique for in situ single cell gene expression analysis. The developed bench-top instrument utilized modified AFM coaxial probes for the extraction of intracellular molecules from cell samples. The adherent cell samples were cultured on collagen gel for select-and-probe analysis. The AFM coaxial probe served as nanotweezer, and wherein the application of an alternating potential between the inner and outer electrodes of the co-axial cable creates a dielectrophoretic force for attracting target molecules toward the tip-end. The technology we described directly targeted mRNA expression levels down to less than 100 molecules within a single living cell without the need for purification and averaging typically of conventional techniques. Target

molecules were extracted from sample cells upon successfully access cell content without cell lysing and affecting cell viability, rendered sample preservation capability for post analysis process. The target cell viability was preserved for the possible post-probing process. We have demonstrated the ability to probe the same sample cell for the second time and thus opened the access for dynamic gene expression study; it might need to investigate applying our technique in some important biological applications.

For samples of suspension cells for cell lines, we developed another approach consisted of a microfluidic lab-on-a-chip platform for high throughput single-cell trapping, integrated with a modified AFM nanoprobing system for the extraction of intracellular molecules from a single cell. The on-chip in situ probing and analysis technique rendered no need of releasing target samples as well as the potential cell loss associated with this process. Also, our method required no cell lysing, and purifications for gene expression analysis, possible material losses for rare samples during these processes were further eliminated. In this process, suspended cell samples were introduced to a microfluidic chip sealed with ultra thin PDMS (Polydimethylsiloxane) membrane, in which individual cells were trapped as a single-cell array for probing. The AFM coaxial probe was modified as nanotweezer, and wherein the application of an alternating potential between the inner and outer electrodes of the co-axial cable created a dielectrophoretic force for attracting target molecules toward the tip-end. The ultra-thin PDMS sealing membrane opened the access of the external micro-manipulating device, here AFM nanoprobes and

similarly micropipette and microinjectors, to the material content inside microfluidic chips, provided potentially analysis and reactions of existing lab-on-a-chip systems with external accessibility and spatial selectivity. The target cell viability was preserved with small probing voltage for possible further downstream process and study. A disadvantage of the platform was that each nanoprobe was only responsible for one sample reading. We are now working on combining target droplet releasing platform, and potentially utilizing well-defined coordinates of target sites of trapping device, integrating the process in a high-throughput manner with system automation. It might also be needed to investigate our platform with real patient samples for the demonstration of CTCs heterogeneity detection, although it seems straight forward from current illustration.

6.2 Concluding Remarks

A major challenge in cancer treatment has been the difficulty in translating findings from studies in relatively homogenous immortalized cell lines and animal models to the clinic. One underlying reason for this is the tremendous genetic heterogeneity both in cells within a tumor, as well as between tumors from different individuals. This is true even if tumors have similar histology and are derived from patients with apparently identical clinical histories. The nanoprobe platform could potentially provide the capability to dynamically assay gene expression profiles of individual cells and cell types in a tumor and to follow the responses to altered environmental conditions and drug regimens. For single cell diagnostics such as

CTC analysis, the developed platform provided no need of depleting white blood cell prior to molecular testing to reduce the possibility of false negative results, as is currently achieved by selectively releasing and harvesting target cells after CTCs enrichment in other groups. The on-chip in situ probing and analysis technique rendered no need of releasing target samples as well as the potential cell loss associated with this process. This is a remarkable improvement as CTCs may exist in low numbers with certain patients' profiles. Moreover, target cell viability is preserved with low probing voltage for possible further downstream process and study. Combine current labeling technique for target cell identification with sufficient probing selection and drug response analysis; our platform provides a possibility for real-time CTC analysis that will bring much needed valuable information on the possible development of drug resistance over the course of anticancer therapy. As CTCs also showed markedly different gene expression profiles compared with those in single cells from cancer cell lines, CTC analysis might complement cell-line analysis in drug development.

The ability to quantify mRNA transcripts as a function of space and time was not available to the biologists. This system directly targets and samples down to a few molecules within a single living cell, without the need for purification and averaging typically of conventional technologies. By providing reliable and exceptional sensitivity to identify differences between individual cells in a seemingly homogeneous population, the system creates possibilities for assaying the genomic analysis in living cells and tracking them in response to external stimuli. This

technique has potential impacts on understanding the heterogeneity of transcriptional responses and its implications for cell function and disease, as well as epigenetic regulation, stem cell development, and cancer research.

REFERENCE

[1] Kalisky T., Blainey P., Quake S., Annu.Rev.Genet., 45: 431-45 (2011)
[2] Wang Y., Mijares M., Gall M.D., Turan T., Javier A., Bornemann D.J., Manage K., Warrior R., Dev Dyn. 239: 2813 (2010)
[3] Paulsson J., Nature. 427: 415 (2004)
[4] Elowitz M.B., Levine A.J., Siggia E.D., Swain P.S., Science. 297:1183 (2002)
[5] Carlo D.D. and Lee L.P., Analytical chemistry. 78: 7918 (2006)
[6] Lecault V., White A.K., Singhal A. and Hansen L.C., Current Opinion in Chemical Biology, 16: 381-390 (2012)
[7] Walling M.A. and Shepard J.R., Chem Soc Rev 40(7): 4049 (2011)
[8] Cohen A.A, et al. Science 322(5907): 1511-1516 (2008)
[9] White A.K., et al. Proc Natl Acad Sci USA 108(34):13999 (2011)
[10] Lawrence M.S., Stojanov P., Polak P., et al. Nature 499(7457): 214 (2013)
[11] Kandoth C., McLellan M.D., Vandin F., et al. Nature 502(7471): 333 (2013)
[12] Alberter B., Klein C.A. and Polzer B. Expert Review of Molecular Diagnostics 16(1): 25-38 (2016)
[13] Bernards R., Weinberg R.A., Nature 418(6900): 823 (2002)
[14] Pantel K., Brakenhoff R.H. Nat. Rev. Cancer 4(6):448 (2004)
[15] Alix-Panabières C. and Pantel K., Clin Chem 59(1):110 (2013)
[16] Riethdorf S., et al. Clin Cancer Res 13(3):920 (2007)
[17] Nagrath S., et al. Nature 450(7173):1235 (2007)
[18] Stott S.L., et al. Proc Natl Acad Sci USA 107(43):18392 (2010)
[19] Saliba A.E., et al. Proc Natl Acad Sci USA 107(33):14524 (2010)
[20] Talasaz A.H., et al. Proc Natl Acad Sci USA 106(10):3970 (2009)
[21] Lee M.G., Shin J.H., Bae C.Y., Choi S., and Park J.K., Anal Chem 85(13):6213 (2013)
[22] Bhagat A.S., Hou H.W., Li L.D., Lim C.T., and Han J. Lab Chip 11(11):1870 (2011)
[23] Lecault V., White A.K., Singhal A., and Hansen C.L., Curr Opin Chem Biol 16(3):381 (2012)
[24] Klein A.M., et al. Cell 161(5):1187 (215)
[25] Chung K., Rivet C.A., Kemp M.L., and Lu H., Anal Chem 83(18):7044 (2011)
[26] Kim, J., Jensen, E.C., Megens, M., Boser, B., and Mathies, R. A., LOC, 11 (18): 3106 (2011)
[27] Toriello, N. M., Douglas, E. S., Thaitrong, N., Hsiao, S. C., Francis, M. B., Bertozzi, C. R. and Mathies, R. PANS 105: 20173 (2008)
[28] Marcus J.S., Anderson W.F., Quake S.R., Anal. Chem. 78: 3084 (2006)
[29] Nagrath S., Sequist L.V., et al. Nature 450 (7173):1235 (2007)
[30] Saliba A.E., Saias L., et al. Proc Natl Acad Sci USA 107 (33):14524 (2010)
[31] Talasaz A.H., Powell A., et al. Proc Natl Acad Sci USA 106(10): 3970 (2009)
[32] Casavant B.P., Mosher R., et al. J. Methods 64(2): 137 (2013)
[33] Lee H.J., Oh J.H., et al. Angew. Chem., Int. Ed. 52(32): 8337 (2013)

[34] Hou H.W., et al. Sci. Rep. 3:1259 (2013)
[35] Karabacak N.M., et al. Nat. Protocols 9(3): 694 (2014)
[36] Mach A.J., Kim J.H., et al. Lab Chip 11(17): 2827 (2011)
[37] Punnoose E.A., et al. PLoS One 5(9): e12517 (2010)
[38] Lohr J.G., Adalsteinsson V.A., et al. Nature Biotechnology 32(5): 479 (2014)
[39] Powell A.A., Talasaz A.H., et al. PLoS ONE 7(5): e33788 (2012)
[40] Blassl C., et al. Mol Oncol S1574-7891(16): 30017 (2016)
[41] Neumann M.H.D, Schneck H., et al. Biotechnol Progress. doi: 10.1002/btpr.2294 (2016)
[42] Yeo T., Tan S.J., et al. Sci. Rep. 6:22076 (2016)
[43] Swennenhuis J.F., Reumers J., et al. Genome Med 5(11):106 (2013)
[44] Rico F., Chu C., et al. Biophys. J. 99:1387 (2010)
[45] Dey S.S., Kester L., et al. Nat Biotechnol 33: 285 (2015)
[46] Stoecklein N.H., et al. Cancer Cell 13: 441 (2008)
[47] Hou S, Zhao L, et al. Angew. Chem. Int. Ed. 52: 3379 (2013)
[48] Pohl H.A., Dielectrophoresis: the Behavior of Neutral Matter in Nonuniform Electric Field, Cambridge University Press, Cambridge, UK (1978)
[49] Huang Y., Joo S., Duhon M., Heller M., Wallace B. and Xu X., Anal. Chem. 74: 3362 (2002)
[50] Doh I. and Cho Y.H., Sensors and Actuators A 121: 59 (2005)
[51] Zheng L., Brody J.P. and Burke P.J., Biosensors and Bioelectronics 20: 606 (2004).
[52] Ermolina I., Milner J. and Morgan H., Electrophoresis 27: 3939 (2006).
[53] Tuukkanen S., Kuzyk A., Toppari J.J., Hytönen V.P., Ihalainen T., and Torma P., Appl. Phys. Lett. 87: 183102 (2005).
[54] Kuzyk A., Burke B., Toppari J.J., Linko V. and Torma P., Small 4: 447 (2008).
[55] Bakewell D.J. and Morgan H., IEEE transactions on nanobioscience 5: 1 (2006).
[56] Ibsen S., Sonnenberg A., Schutt C., Mukthavaram R., Yeh Y., Ortac I., Manouchehri S., Kesari S., Esener S., and Heller M.J., Small, 11(38): 5088 (2015)
[57] Suzuki S.; Yamanashi T.; Tazawa S.; Kurosawa O.; Washizu M. IEEE Trans. Ind. Appl. 34 (1): 75 (1998)
[58] Cheng J., Sheldon E. L., Wu L., Uribe A., Gerrue L.O., Carrino J., Heller M.J., O'Connell J.P., Nat. Biotechnol. 16: 541 (1998)
[59] O'Konski C.K., J. Phys. Chem. 64: 605 (1960).
[60] Ermolina I., Morgan H., Journal of Colloid and Interface Science 285: 419 (2005)
[61] Holze R., IET Nanobiotechnol., 3 (2): 28 (2009)
[62] Martin Y., Williams C.C. and Wickramasinghe H.K., J. Appl. Phys. 61: 4723 (1987)
[63] Binnig G., Quate C.F., and Gerber C.H., Phys. Rev. Lett. 56: 930 (1986)
[64] Salaita K., Wang Y., and Mirkin C.A., Nat. Nanotechnol. 2: 145 (2007)
[65] Xie H., Haliyo D.S., and Régnier S., Nanotechnology 20: 215301 (2009)

[66] Dorig P., Stiefel P., Behr P., Sarajlic E., Bijl D., Gabi M., Vörös J., Vorholt J.A. and Zambelli T., Appl. Phys. Lett. 97: 023701 (2010).
[67] Orane G.G., et.al. Trends in Biotechnology, 32(7): 381 (2014)
[68] Seiji A., et al. Applied Physics Letters 79: 1691 (2001)
[69] Rosner B.T.; Bork T.; Agrawal V.; Weide D.W, Sens. Actuators A, 102: 185 (2002)
[70] Noh J.H., Nikiforov M., Kalinin S.V., Vertegel A.A., Rack P. D. Nanotechnology 21: 365302 (2010)
[71] Brown K.A., Aguilar J.A. and Westervelt R.M., Applied Physics Letters 96: 123109 (2010)
[72] Brown K.A. and Westervelt R.M., Nano Lett. 11: 3197 (2011)
[73] Brown K.A., Berezovsky J. and Westervelt R.M., Applied Physics Letters 98: 183103 (2011)
[74] Basuray S. and Chang H.C., Phys. Rev. E 75: 060501 (2007)
[75] Ermolina I. and Morgan H., Journal of Colloid and Interface Science 285: 419 (2005)
[76] Bonincontro A., Mari C., Mengoni M. and Risuleo G., Biophys. Chem. 67: 43 (1997)
[77] Gadani D.H., Rana V.A., Bhatnagar S.P., Prajapati A.N. and Vyas A.D., Indian J. Pure Appl. Phys. 50: 405 (2012).
[78] Clarke W., Piper J.D., Ying L. and Klenerman D., Phys. Rev. Lett. 98: 198102 (2007).
[79] Tsoi M., Biophysical Chemistry 147: 104 (2010).
[80] Adenier A. and Aaron J.J., Spectrochimica Acta Part A 58: 543 (2002).
[81] Rahimi Y., Goulding A., Shrestha S., Mirpuri S. and Deo S.K., Biochem Biophys Res Commun. 370: 57 (2008).
[82] Tuukkanen S., Toppari J., Kuzyk A., Hirviniemi L., Hytönen V.P., Ihalainen V. and Törmä P., Nano Lett. 6: 1339 (2006)
[83] Spanakis E.. Nucleic Acids Res 21:3809 (1993)
[84] Thellin O., Zorzi W., Lakaye B., DeBorman B., Coumans B., Hennen G., Grisar T., Igout A, Heinen E., J Biotechnol 75:291 (1997)
[85] Shapiro E., Biezuner T. and Linnarsson S., Nature Reviews Genetics, 14: 618 (2013)
[86] Streets A.M., Zhang X., Cao C., Pang Y., Wu X., Xiong L., Yang L., Fu Y., Zhao L. and Tang F., Proceedings of the National Academy of Sciences, 111: 7048 (2014)
[87] Sanchez-Freire V., Ebert A.D., Kalisky T., Quake S.R. and Wu J.W., Nature Protocols, 7: 829 (2012)
[88] Macosko E.Z., Basu A., Satija R., Nemesh J., Shekhar K., Goldman M., Tirosh I., Bialas A.R., Kamitaki N. and Martersteck E.M., Cell, 161: 1202 (2015)
[89] Chung K., Rivet C.A., Kemp M.L., and Lu H. Analytical Chemistry 83(18):7044 (2011)
[90] Thangawng A.L., Swartz M.A., Glucksberg M.R. and Ruoff R.S., Small, 3: 132 (2007)

[91] Thangawng A.L., Ruoff R.S., Swartz M.A. and Glucksberg M.R., Biomedical Microdevices, 9: 587 (2007)
[92] Wagner I., Materne E.M., Brincker S., Suessbier U., Fraedrich C., Busek M., Sonntag F., Sakharov D.A., Trushkin E.V., Tonevitsky A.G., Lauster R. and Marx U., Lab on a Chip, 13: 3538 (2013)
[93] Punnoose E.A., Atwal S.K., Spoerke J.M., Savage H., Pandita A., Yeh R.F., Pirzkall A., Fine B.M., Amler L.C. and Chen D.S., PloS one, 5: e12517 (2010)
[94] Roussidis A., Theocharis A., Tzanakakis G. and Karamanos N., Current medicinal chemistry, 14: 735 (2007)
[95] Stonehouse T., Woodhead V., Herridge P., Ashrafian H., George M., Chain B. and Katz D., Immunology, 96: 35 (1999)
[96] Lorenzi T., Turi A., Lorenzi M., Paolinelli F., Mancioli F., Sala L., Morroni M., Ciarmela P., Mantovani A. and Tranquilli A.L., PloS one, 7: e35232 (2012)
[97] Karagiannis P., Singer J., Hunt J., Gan S.K.E., Rudman S.M., Mechtcheriakova D., R. Knittelfelder R., Daniels T.R., Hobson P.S., Beavil A.J., Spicer J., Nestle F.O., Penichet M.L., Gould H.J., Jensen-Jarolim E. and Karagiannis S.N., Cancer Immunology Immunotherapy 58: 915 (2009)
[98] Thomsen E.R., Mich J.K., Yao Z., Hodge R.D., Doyle A.M., Jang S., Shehata S.I., Nelson A.M., Shapovalova N.V., Levi B.P.and Ramanathan S., Nature Methods, 13: 87 (2016)

APPENDIX A: PCR PRIMER DESIGN

The mRNA sequences of ACTB, GAPDH, HPRT, CD45, EpCAM, and HER2 were checked in GenBank, and their primers were designed using the online PrimerQuest® Tool (Integrated DNA Technologies). All the primers were designed to be intron-spanning to preclude amplification of genomic DNA. The sequences of the above primers were as follows:

ACTB, 5'-TCATCACCATTGGCAATGAG-3' (forward) and 5'-ACTCCATGCCCAGGAAGGA-3' (reverse);

GAPDH, 5'-TCCACTGGCGTCTTCACC-3' (forward) and 5'-GGCAGAGATGATGACCCTTTT-3' (reverse);

HPRT, 5'-TGACCTTGATTTATTTTGCATACC-3' (forward) and 5'-CGAGCAAGACGTTCAGTCCT-3' (reverse);

CD45, 5'-CGGCTGACTTCCAGATATGAC-3' (forward) and 5'-GCTTTGCCCTGTCACAAATAC-3' (reverse);

EpCAM, 5'- CGCAGCTCAGGAAGAATGTG-3' (forward) and 5'-TGAAGTACACTGGCATTGACG-3' (reverse);

HER2, 5’-AAAGGCCCAAGACTCTCTCC-3’ (forward) and 5’-CAAGTACTCGGGGTTCTCCA-3’ (reverse).

All the primers were purchased from Integrated DNA Technologies. DNA oligomers (Integrated DNA Technologies) with same sequences as the target genes’ amplicons were used to construct standard curves for the calibration of molecule numbers from RT-qPCR results.

APPENDIX B: SILANE CHEMISTRY BASED PEGYLATION PROCEDURE

Cleaning

1. Rinse the fabricated coaxial probes in acetone for 10mins
2. Rinse the sample in Iso-Propyl Alcohol for 2-5mins
3. Rinse in running deionized or Millipore water
4. Air dry for 20min

UV Treatment

1. Treat cleaned samples in UV ozone for 90mins

PEG modification

1. Incubate in 2%(v/v) 2-[Methoxy(polyethyleneoxy)propyl] trimethoxysilane (PEG-Silane) in 100% toluene for 3hrs at 60 °C on hot plate. The beaker (glass or polypropylene) was sealed with parafilm.
2. Rinse in Sequentially in Toluene, Ethanol, and water.
3. Bake on hotplate 110C - 15mins

The PEGylation reaction was characterized by measuring the water contact angle on a SiO_2 surface. The contact angle was estimated to be approximate 37˚